

B3 0003+387: AGN Marked Large-Scale Structure at Redshift 1.47? ^{1,2}

D. Thompson

Palomar Observatory, California Institute of Technology

MS 320-47, Pasadena, CA 91125

djt@mop.caltech.edu

O. Aftreth

California Institute of Technology

MS 175-48, Pasadena, CA 91125

and

B. T. Soifer³

Palomar Observatory, California Institute of Technology

MS 320-47, Pasadena, CA 91125

ABSTRACT

We present evidence for a significant overdensity of red galaxies, as much as a factor of 14 over comparable field samples, in the field of the $z = 1.47$ radio galaxy B3 0003+387. The colors and luminosities of the brightest red galaxies are consistent with their being at $z > 0.8$. The radio galaxy and one of the red galaxies are separated by 5'' and show some evidence of a possible interaction. However, the red galaxies do not show any strong clustering around the radio galaxy nor around any of the brighter red galaxies. The data suggest that we are looking at a wall or sheet of galaxies, possibly associated with the radio galaxy at $z = 1.47$. Spectroscopic redshifts of these red galaxies will be necessary to confirm this large-scale structure.

Subject headings: galaxies: clusters: general — galaxies: distances and redshifts — large-scale structure of universe — infrared: galaxies

1. Introduction

As the most massive collapsed objects in the universe, clusters provide a sensitive probe

¹This paper uses data obtained at the WIYN Observatory, a joint facility of the University of Wisconsin-Madison, Indiana University, Yale University, and the National Optical Astronomy Observatories.

²Based in part on observations obtained at the W. M. Keck Observatory.

³Also at the SIRTF Science Center, California Institute of Technology, Pasadena, CA 91125

of the formation and evolution of structure in the universe. The presence of clusters or large-scale structure at and beyond $z \approx 1$ can constrain scenarios for bottom-up structure formation and fundamental cosmological parameters like Ω_0 by requiring cluster-level collapse earlier than was previously thought possible. Study of the individual galaxies in high- z clusters can also provide information on the cluster environment, merging and star formation history in the cluster galaxies, and samples of cluster ellipticals and spirals which could be compared with field galaxies at the same redshift.

A number of confirmed or suspected clusters are known at redshifts above one, with some candidates extending up to $z \sim 3$ (see Postman (2000) for a recent review). These include clusters around or foreground to high- z active galactic nuclei (Le Fevre et al. 1996; Malkan, Teplitz, & McLean 1996; Dickinson 1997; Hall & Green 1998; Clements 2000; Tanaka et al. 2000; Liu et al. 2000), a near-infrared selected cluster (Stanford et al. 1997), a cluster associated with correlated quasar absorption line systems (Francis et al. 1996), X-ray selected clusters (Rosati et al. 1999; Hasinger et al. 1998), Lyman break galaxies (Steidel et al. 1998), and a distant cluster which gravitationally lenses a background QSO (Benitez et al. 1999).

Identifying structures directly in visual wavelength data becomes increasingly difficult at $z \gtrsim 1$. The fainter galaxies and strong cosmological K-corrections serve to reduce the contrast of the high- z galaxies against the dense background of faint blue field galaxies at visual wavelengths. The contrast at near-infrared wavelengths, however, remains high even at $z \gtrsim 1$ because the K-corrections are lower and well-behaved.

In most high-redshift clusters, there is a clear concentration of the galaxies around what would be considered a classical cluster

“core,” though Hall & Green (1998) find some evidence for overdensities of red objects lacking a central concentration in fields of $z \sim 1.5$ radio-loud quasars. The structures found by Steidel et al. (1998) and Francis et al. (1996) are extended over large regions of sky. These fields may actually be sampling sheets or filaments of galaxies associated with large-scale structure, or perhaps a protocluster seen in a dynamically young state, before any significant virialization has occurred.

In this paper we present optical and near-infrared observations of a high redshift radio galaxy field, covering a total area of 44.3 sq. arcmin, where an overdensity of red galaxies suggests the presence of some large-scale structure, perhaps a wall or sheet of galaxies rather than a collapsed cluster.

2. Observations and Reductions

B3 0003+387 is a 1.36 Jy radio source at 408 MHz in the Third Bologna Survey (Ficarra, Grueff, & Tomassetti 1985). The source is unresolved with 15'' resolution at 1.4 GHz (Vigotti et al. 1989). An optical spectrum obtained by Djorgovski et al. (priv. comm.) indicates a redshift of 1.47, with strong emission lines typical for powerful radio galaxies. Preliminary images at optical and near-infrared wavelengths of the B3 0003+387 field identified a number of very red galaxies near the radio source, possibly indicating the presence of a high redshift cluster, and prompting the deeper observations presented in this paper. All reductions were performed using standard IRAF⁴ (Tody 1993) commands.

⁴IRAF is distributed by the National Optical Astronomy Observatories, which are operated by the Association of Universities for Research in Astronomy, Inc., under cooperative agreement with the National Science Foundation.

2.1. K' -Band Imaging

The K' data were obtained on UT 1997 June 20 using the Omega-Prime camera (Bizenberger et al. 1998) at the Calar Alto 3.5 m telescope in Spain. Omega-Prime is a direct imaging camera with no cold pupil stop, imaging onto a HAWAII 1024² HgCdTe array. The image scale is 0''.396/pixel, giving an unvignetted field of view 6''.75 square. We obtained 58 images in a random offset pattern designed to maximize the pointing separation between temporally adjacent images. Each image was the sum of ten 3-second integrations, giving a total exposure time of 29 minutes.

We reduced the data using IRAF and a double-pass reduction algorithm. After a first pass of sky-subtraction and flatfielding, residual gradients in the background were removed in the second pass using object masks to explicitly ignore pixels covered by known objects and bad pixels. The reduced images were resampled to 2048² pixels prior to integer pixel offsets and stacking, giving a final pixel scale very close to that of the WIYN data (0''.198 vs. 0''.195).

The data were calibrated onto the Vega scale using several stars from the UKIRT faint standards list (Casali & Hawarden 1992). The night was not strictly photometric, but internal consistency of the standard star measurements indicate that the systematic uncertainty in the calibration is below 10%. The final K' image has a full-width at half-maximum (FWHM) of 1''.1, and a 5-sigma point source detection limit within an aperture diameter equal to twice the seeing (2''.2) of $K' = 20.31$. A two arcminute square subsection of the K' image, centered on the radio galaxy, is shown in the left panel of Figure 1.

2.2. R -Band Imaging

Deep R -band data of the B3 0003+387 field were obtained through service observing with the CCD imager at the 3.5m WIYN telescope on UT 1997 August 01 and UT 1997 August 05 in non-photometric but good seeing conditions. The imager uses a 2048² pixel CCD with an effective plate scale of 0''.195 per 21 μ m pixel, giving a 6''.66 square field of view which is well matched to the near-infrared image. The data were taken through a Harris R filter, which has a central wavelength of 646 nm and a FWHM of 153 nm. A series of short exposures of the B3 0003+387 field and the Landolt (1992) standard fields SA92, SA110-L1 and Mark A were later obtained with the same instrument under nearly photometric conditions on UT 1997 October 12 for calibration.

Standard CCD processing was used to remove the bias and flatfield each image. Because the eight deep images were obtained on two different nights and under varying conditions, the signal-to-noise ratio (SNR) varies slightly from image to image. We normalized the object photometry across all images, then derived weights proportional to the variance in the rescaled sky background. These eight rescaled images were then combined with variance weighting, using cosmic ray and bad pixel masks.

The calibration of the deep R image was transferred from the shallower data taken on a nearly photometric night. The standards indicate a stable night with $\sim 0^m 17$ magnitudes of extinction over that expected under truly photometric conditions. The final R -band image has a FWHM of 0''.8, and a 3-sigma point source detection limit within an aperture diameter equal to twice the seeing (1''.6) of $R_{Harris} = 25.58$. A two arcminute square subsection of the R image, centered on the radio galaxy, is shown in the right panel of Figure 1.

2.3. Keck K -Band Imaging

A deeper broadband K image of the area around the radio galaxy was obtained on UT 1997 August 20 using NIRC (Matthews & Soifer 1994) on the Keck I telescope. NIRC reimaged the infrared f/25 Keck focal plane onto a 256² Indium Antimonide detector at 0''.15 per pixel, for a 38''.4 square field of view. We obtained a total of 29 1-minute integrations, most in a regular 3×3 pattern with 5'' spacing. Individual images consist of a sum of six 10-second exposures.

Images were first sky-subtracted with a median stack of six to eight dithered images in the same field, then flatfielded with a skyflat derived from the same data. The reduced images were combined with integer pixel offsets. The data were calibrated onto the Vega scale using the Persson et al. (1998) infrared standard stars. The night was relatively stable but not strictly photometric. We estimate the systematic uncertainty in the zero point is again below 10%. The K -band image has a FWHM of 0''.42, and a 5-sigma point-source detection limit in the deep central part of the image of $K = 22.44$. The K -band image and corresponding area of the R -band image are shown in Figure 2.

2.4. Astrometry

Hubble Space Telescope Guide Star Catalog (GSC⁵) stars around B3 0003+387 were used to derive fainter secondary position standards on a Digitized Sky Survey⁶ image of the field. The absolute uncertainties in the astrometric solutions are $\Delta \approx 0''.3$ in both the R and K' images. Objects in the Keck K -band image were matched to the R and K' images

⁵GSC: Produced at the Space Telescope Science Institute under U.S. Government grant.

⁶DSS: Made by the California Institute of Technology with grants from the National Geographic Society, and produced at the Space Telescope Science Institute.

by hand and were not fit with an astrometric solution.

The near-infrared object corresponding to B3 0003+387 was found to be at $00^h 06^m 20\rlap{.}^s.71 +39^\circ 00' 28\rlap{.}''1$ (J2000). This agrees ($\Delta\alpha = 0''.0$, $\Delta\delta = 1''.1$) to well within the positional uncertainties from the VLA in C-configuration at 1.4 GHz (FWHM = 15''), used for the B3VLA Survey (Vigotti et al. 1989). This is also the object for which Djorgovski et al. (priv. comm.) obtained the $z = 1.47$ redshift. We therefore consider this identification of the radio galaxy secure.

2.5. Object Catalog

We created a catalog of all objects detected in the K' image, and used the APPHOT package in IRAF to extract the magnitudes within a 4'' diameter aperture. In a small number of cases, the photometry for close pairs or multiples was extracted by hand after subtracting out the contaminating objects. The APPHOT positions in the K' image were transformed into coordinates on the R image using our astrometric solution, and the corresponding R -band magnitudes extracted. Any K' -selected objects that were not detected in R were assigned the three-sigma limit of $R = 25.58$. Because the R image is much deeper than the K' image, there are large numbers of faint, relatively blue objects detected in the R image which do not have a corresponding detection in the K' and therefore do not appear in the object catalog.

The final catalog (Table 1) contains the K' and R centroids, magnitudes, uncertainties on the magnitudes (statistical only), and J2000 coordinates for all K' -selected objects covering an area of 44.3 square arcminutes, or 1.23×10^{-2} square degrees. There are 421 objects in the catalog, although 4 were deleted because of unrecoverable contamination in the R image. The catalog and survey images are available through the electronic version of the

3. Discussion

In the absence of spectroscopic redshifts for these red galaxies, we must rely on the imaging and photometry in hand to determine if there is a cluster or some sort of large-scale structure present in this field. Specifically, we address the overdensity of red objects in the field relative to a field sample, the spatial distribution of these red objects, and what their redshift might be.

We use the data from two widely-separated fields obtained as part of the Calar Alto Deep Imaging Survey (CADIS; see Meisenheimer et al. (1997) for a description of the survey) as a control sample for comparison to the B3 data. The CADIS fields were chosen to be “blank” fields at high galactic latitude, free of bright stars or galaxies, as well as known galaxy clusters and therefore should be representative of the field population of red objects. Each field is ~ 3 times the area of our data, and the combined area covers 6.4 times the area of the B3 0003+387 field. The CADIS and B3 infrared data were obtained with the same instrument. Both datasets use non-standard R -band filters, but the differences are negligible and the two data sets are directly comparable. Thompson et al. (1999) presented initial results on the surface density of field extremely red galaxies from the CADIS data.

For the following discussion, we assume that all of the red objects in the radio galaxy field are galaxies. Most ($\sim 75\%$) are resolved in the infrared image, but contamination of the sample by low mass stars, from late M dwarfs through L and T type brown dwarfs, is still possible. Our survey field has a relatively high galactic latitude ($l_{II} = 113^\circ, b_{II} = -23^\circ$) and only covers a volume of 1.25 pc^3 to a distance of 100 pc. We expect much less than one low mass star within this volume, given recent

determinations of their space density (Reid et al. 1999; Herbst et al 1999).

3.1. An Excess of Red Galaxies

A color-magnitude diagram for the B3 0003+387 field is shown in Figure 3. We also plot the median and $\pm 1.75\sigma$ distribution of colors from Thompson et al. (1999), derived from the CADIS data. Several features in Figure 3 are immediately obvious. First, there are a number of objects with blue colors ($(R - K') < 2^m$) which span the full range of K' magnitudes. These are typically galactic subdwarf stars. Second, no objects brighter than $K' = 17.5$ appear redder than the $+1.75\sigma$ line. However, this is consistent with purely statistical fluctuations, as only 4 objects would be expected to lie at $> 1.75\sigma$ in our sample of 108 with $K' < 17.5$. Finally, there are a large number of objects with $K' > 17.5$ and redder than the $+1.75\sigma$ line.

Is this excess of red galaxies in the B3 0003+387 field significant? We compared the surface density of galaxies in the B3 field with the combined control fields from CADIS to determine the overdensity. We first selected galaxies from both sets of data in the $17.0 \leq K' \leq 19.0$ magnitude range. This covers the relevant range for the red galaxies while avoiding problems with incompleteness at fainter magnitudes. We then sampled the data in 1 magnitude bins of color, spaced every half magnitude. Adjacent bins therefore are *not* statistically independent. We show in Figure 4 the logarithm of the surface density of galaxies in the two sets of data as a function of the $(R - K')$ color, *normalized* by the CADIS data. The 1σ uncertainties from Poisson counting statistics are also indicated.

While the surface densities in the two fields agree to within the uncertainties for $(R - K') \leq 5^m$, there is a significant excess of galaxies at redder colors. The most significant bin, with a 3.7σ excess, is at $(R - K') = 6^m$ (cov-

ering the range $5^m5 \leq (R - K') \leq 6^m5$. The highest overdensity of red galaxies occurs at $(R - K') = 7^m$. Combining the overdensities in statistically independent bins shows a $\sim 4.5\sigma$ excess for $(R - K') \geq 5^m5$. This suggests that this B3 field is not representative of the general field population, and that there is a large overdensity of red galaxies in this field.

This overdensity of red galaxies may indicate the presence of a high redshift cluster, but there is no clear red sequence (Bower, Lucey, & Ellis 1992a,b) of cluster ellipticals visible in the color-magnitude diagram (Figure 3). We next consider the spatial distribution of these red galaxies in the B3 field.

3.2. Red Galaxy Spatial Distribution

Our survey field covers $6'46 \times 6'86$. For an Einstein-de Sitter Universe ($\Omega_M = 1$, $\Omega_\Lambda = 0$; with $H_0 = 100h \text{ km s}^{-1} \text{ Mpc}^{-1}$) at the redshift of the radio galaxy, this translates to a field of $1.66h^{-1} \text{ Mpc} \times 1.76h^{-1} \text{ Mpc}$, considerably larger than a typical galaxy cluster core. If an evolved, relaxed cluster were in our field, we would expect to see a significant concentration of galaxies around the cluster core.

For purposes of the discussion in this section, it is useful to divide up the group of red galaxies into three subsets: the brightest red galaxies, the extremely red objects, and the red excess galaxies. We show these subsets graphically in Figure 5, which reproduces the faint red end of the color-magnitude diagram (Figure 3) in greater detail.

The brightest red galaxies (BRGs) subset consists of the 11 galaxies with $17.5 \leq K' \leq 18.3$ and $5^m2 \leq (R - K') \leq 5^m8$ in the B3 0003+387 field. Eight of these are resolved in the infrared image. Such a group of objects with similar magnitudes and colors suggests that they may have a similar evolutionary history, possibly associated in a cluster. In addition, their redder than normal colors imply

that these BRGs are likely to be at high redshift.

The extremely red galaxies (ERGs) subset includes 20 galaxies with $(R - K') \geq 6^m0$ and $K' \leq 19.0$, adopting the definition from Thompson et al. (1999). Fifteen of these ERGs are resolved. The B3 0003+387 field covers 44.3 square arcminutes of sky, giving a local surface density for the ERGs of $0.45 \pm 0.10 \text{ arcmin}^{-2}$, a factor of ~ 12 higher than that found in the CADIS data (Thompson et al. 1999).

The red excess galaxies (REGs) subset is defined as the galaxies with an $(R - K')$ color greater than $+1.75\sigma$, where the mean color and uncertainty are taken from Thompson et al. (1999). This sample includes both the BRG and ERG subsets. For ease of use, we approximate the $+1.75\sigma$ limit with the relation: $(R - K') \geq 0.735 K' - 8.23$ for $K' > 18^m$, and $(R - K') \geq 5$ for $K' \leq 18^m$.

The spatial distribution of these subsets is shown in Figure 6, where we plot the positions of all objects in the B3 0003+387 field, highlighting the three subsets defined above. What is immediately obvious in this plot is that there is no strong concentration of red galaxies around B3 0003+387. This is in marked contrast to other high redshift clusters studied in the near infrared (Stanford et al. 1997; Rosati et al. 1999). We note that the infrared data around those clusters is considerably deeper ($1^m5 - 2^m0$) than here and thus would be able to select cluster galaxies significantly further down the luminosity function. Our data do not provide evidence that B3 0003+387 lies in the core of a high-redshift cluster.

There is a possible concentration of red excess galaxies around one of the BRGs, catalog number 106, located to the northwest of the radio galaxy. This galaxy, with $K' = 18.17$ and $(R - K') = 5^m24$, is not exceptional in our sample: it is the bluest and one of the fainter

galaxies in the BRG subset. There are eight objects from the REG subset, one of which is an ERG, within a circular aperture of $45''$ radius. This is a factor of ~ 3 less than in the Stanford et al. (1997) and Rosati et al. (1999) clusters, assuming all of the red excess galaxies are associated.

In order to place more quantitative limits on the concentration of galaxies around any galaxies in our field, we investigated the radial surface density distribution of red galaxies with respect to various reference objects (BRGs and ERGs). In no case was there a statistically significant overdensity. Figure 7 shows the relative radial surface density of the red excess galaxies around B3 0003+387 and galaxy #106. In both cases, the data are normalized to unity at a radius of two arcminutes. The distribution of red excess galaxies around B3 0003+387 is completely consistent with the bluer field galaxies selected in the same magnitude range. While galaxy #106 does show an overdensity of a factor of six to eight, it is not statistically significant (less than 2σ). Note that both galaxies have other galaxies nearby which skew the results at small radii, but they remain consistent with a uniform surface density to within the uncertainties.

3.3. What is the Redshift?

While there is a significant excess of red galaxies in this field, their distribution on the sky does not support the interpretation that there is a cluster in the B3 0003+387 field. The data are consistent with our looking through a wall or sheet of galaxies. The obvious question is whether this structure is associated with the radio galaxy, or merely a line-of-sight superposition?

A single color ($R - K'$) is not sufficient for more sophisticated photometric redshift fitting, which normally requires photometry through three or more filters. However, even

passively-evolving elliptical galaxy colors do not become particularly red until the normally strong 4000\AA break is redshifted through the R filter, which occurs at $z \simeq 0.8$ for the Harris R filter used in this study. Colors as red as $(R - K') > 5.^m2$, corresponding to the *bluest* of our red excess galaxies, are difficult to explain unless the galaxies are at $z \gtrsim 1$. The characteristics of the filters used in this project, and the resulting very red colors of the galaxies allow us to place a lower limit of $z \geq 0.8$ on their redshift.

We note that it is also possible to produce such red colors in a strong starburst at lower redshift, $z \lesssim 0.5$, assuming heavy extinction from dust. However, the high surface density of red galaxies in this field would be very unusual, given the relatively low fraction of starbursts found in ERGs (Cimatti et al. 1999).

Assuming the red excess galaxies are associated at a common redshift in some sort of wall or sheet structure, the luminosities of the brightest of our red excess galaxies can also place constraints on the redshift. We compare the brightest of our BRG subset, at $K' \sim 17.7$, to the “brightest cluster member” galaxies seen in other high-redshift clusters. These brightest cluster members follow a tight correlation in the K -band Hubble diagram (Collins & Mann 1998; Arag{on}-Salamanca, Baugh, & Kauffmann 1998) up to at least a redshift of one. Comparing our data to other high-redshift clusters (Table 2) shows that we are at least consistent with the $z > 1$ interpretation, and there is sufficient scatter in the K magnitudes that our red excess galaxies could indeed be at $z = 1.47$.

The origin of the activity in the central engines of radio galaxies can often be traced to recent or ongoing mergers. We note that there is a bright and very red galaxy, with $K = 18.36$ and $(R - K) = 5.^m80$ about 5 arcseconds ($\sim 21 h^{-1} \text{kpc}$) east of B3 0003+387.

In the K -band image from Keck (Figure 2), this galaxy shows an asymmetric morphology, visible in the contours, with a spur or elongation in the direction of the radio galaxy. There are additional faint features to the west of the radio galaxy and east of the red galaxy, roughly aligned with the axis between the two galaxies, which may be the visible remnants of tidal tails created by gravitational interaction. However, these features are very faint and may be attributable to image noise or superposition of another object along the line of sight to the radio galaxy. If this interaction is real, then this also supports the interpretation that the red galaxies in the B3 0003+387 field lie at $z = 1.47$, the redshift of the radio galaxy.

4. Summary

We have identified a significant overdensity of red galaxies in an extended field (44.3 square arcmin) around the $z = 1.47$ radio galaxy B3 0003+387. This overdensity is as much as a factor of 14 higher than seen in equivalent blank-field surveys. The spatial distribution of the galaxies is *not* consistent with their being associated in an evolved cluster centered on the radio galaxy, although we believe the evidence does strongly suggest that we are looking through a sheet or wall of galaxies associated with some extended Large-Scale Structure. The red colors of these galaxies are difficult to explain without the large cosmological K-corrections that would come with their being at high redshift ($z > 1$). The presence of a powerful, high-redshift radio galaxy in the field, as well as its possible interaction with one of the red galaxies, suggest that this structure may lie at the same redshift as the radio source: $z = 1.47$.

It will be important to verify the reality of this high-redshift structure by obtaining spectroscopic redshifts for some fraction of the red galaxies in this field. The brightest of the

red excess galaxies are bright enough at visual wavelengths ($R \sim 23\text{--}24^m$) to make spectroscopic followup possible with 8–10 m-class telescopes. In order to facilitate this followup, as well as further study of this field, we are making our full dataset available through the electronic version of the Astronomical Journal.

This project was partially supported by a Caltech Summer Undergraduate Research Fellowship (SURF) for OA. We wish to thank S. Djorgovski for kindly providing the redshift for B3 0003+387, and G. Neugebauer for obtaining the Keck K -band image. The NOAO WIYN-Queue staff did an excellent job of obtaining the R data for this project. We also thank Pat Hall for his helpful comments in refereeing this paper.

REFERENCES

- Aragón-Salamanca, A., Ellis, R. S., Couch, W. J., & Carter, D. 1993, MNRAS, 262, 764
- Aragón-Salamanca, A., Baugh, C. M., & Kauffmann, G. 1998, MNRAS, 297, 427
- Benitez, N., Broadhurst, T., Rosati, P., Courbin, F., Squires, G., Lidman, C., & Magain, P. 1999, ApJ, 527, 31
- Bizenberger, P., McCaughrean, M., Birk, C., Thompson, D., & Storz, C. 1998, in *Astro-nomical Telescopes and Instrumentation*, SPIE conference proceedings, vol. 3354, 825
- Bower, R. G., Lucey, J. R., & Ellis, R. S. 1992a, MNRAS, 254, 589
- Bower, R. G., Lucey, J. R., & Ellis, R. S. 1992b, MNRAS, 254, 601
- Casali, M. M. & Hawarden, T 1992, in *JCMT UKIRT Newsletter*, 4, 33
- Cimatti, A., Daddi, E., di Serego Alighieri, S., Pozzetti, L., Mannucci, F., Renzini, A., Oliva, E., Zamorani, G., Andreani, P. & Röttgering, H. J. A. 1999, A&A, 352, 45
- Clements, D. L. 2000, MNRAS, 312, L61
- Collins, C. A. & Mann, R. G. 1998, MNRAS, 297, 128
- Dickinson, M. 1997, in *HST and the High Redshift Universe*, eds. N. Tanvir, A. Aragón-Salamanca, & J. V. Wall, (World Scientific:Singapore), 207
- Djorgovski, S. et al., unpublished
- Ficarra, A., Grueff, G. & Tomassetti, G. 1985, A&AS, 59, 255
- Francis, P., Woodgate, B., Warren, S., Moller, P., Mazzolini, M., Bunker, A., Lowenthal, J., Williams, T., Minezaki, T., Kobayashi, Y. & Yoshii, Y. 1996, ApJ, 457, 490
- Hall, P. B. & Green, R. F. 1998, ApJ, 507, 558
- Hasinger, G., Giacconi, R., Gunn, J. E., Lehmann, I., Schmidt, M., Schneider, D. P., Truemper, J., Wambsganss, J., Woods, D., & Zamorani, G. 1998, A&A, 340, L27
- Herbst, T. M., Thompson, D., Fockenbrock, R., Rix, H.-W., & Beckwith, S. V. W. 1999, ApJ, 526, 17
- Landolt, A. 1992, AJ, 104, 340
- Le Fevre, O., Deltorn, J. M., Crampton, D., & Dickinson, M. 1996, ApJ, 471, 11
- Liu, M. C., Dey, A., Graham, J. R., Bundy, K. A., Steidel, C. C., Adelberger, K., & Dickinson, M. E. 2000, AJ, in press (astro-ph 0002443)
- Malkan, M. A.; Teplitz, H.; McLean, I. S. 1996, ApJ, 468, L9
- Matthews, K. & Soifer, B.T. 1994, in *Experi-mental Astronomy*, 3, 77
- Meisenheimer, et al. 1997, in *The Early Universe with the VLT*, ed. J. Bergeron (Springer:Heidelberg), 165
- Persson, S. E., Murphy, D. E., Krzeminski, W., Roth, M. & Rieke, M. J. 1998, AJ, 116, 2745
- Postman, M. 2000, in *Clustering at High Redshift*, eds. A. Mazure, O. Le Fevre, & V. Lebrun, (ASP:San Francisco) ASP Conference Series, 200, in press, also astro-ph/9910473

Reid, I. N., Kirkpatrick, J. D., Liebert, J., Burrows, A., Gizis, J. E., Burgasser, A., Dahn, C. C., Monet, D., Cutri, R., Beichman, C. A., & Skrutskie, M. 1999, ApJ, 521, 613

Rosati, P., Stanford, S. A., Eisenhardt, P. R., Elston, R., Spinrad, H., Stern, D., & Dey, A. 1999, AJ, 118, 76

Stanford, S. A., Elston, R., Eisenhardt, P. R., Spinrad, H., Stern, D., & Dey, A. 1997, AJ, 114, 2232

Steidel, C. C., Adelberger, K. L., Dickinson, M., Giavalisco, M., Pettini, M., & Kellogg, M. 1998, ApJ, 492, 428

Tanaka, I., Yamada, T., Aragón-Salamanca, A., Kodama, T., Miyaji, T., Ohta, K., & Arimoto, N. 2000, ApJ, 528, 123

Thompson, D., Beckwith S. V. W., Fockenbrock, R., Fried, J., Hippelein, H., Huang J.-S., von Kuhlmann, B., Leinert, Ch., Meisenheimer, K., Phleps, S., Röser, H.-J., Thommes, E. & Wolf, C. 1999, ApJ, 523, 100

Tody, D. 1993, in *Astronomical Data Analysis Software and Systems II*, eds. R.J. Hanisch, R. J. V. Brissenden, & J. Barnes, A.S.P. Conference Series, 52, 173

Vigotti, M., Grueff, G., Perley, R., Clark, B. G., & Bridle, A. H. 1989, AJ, 98, 419

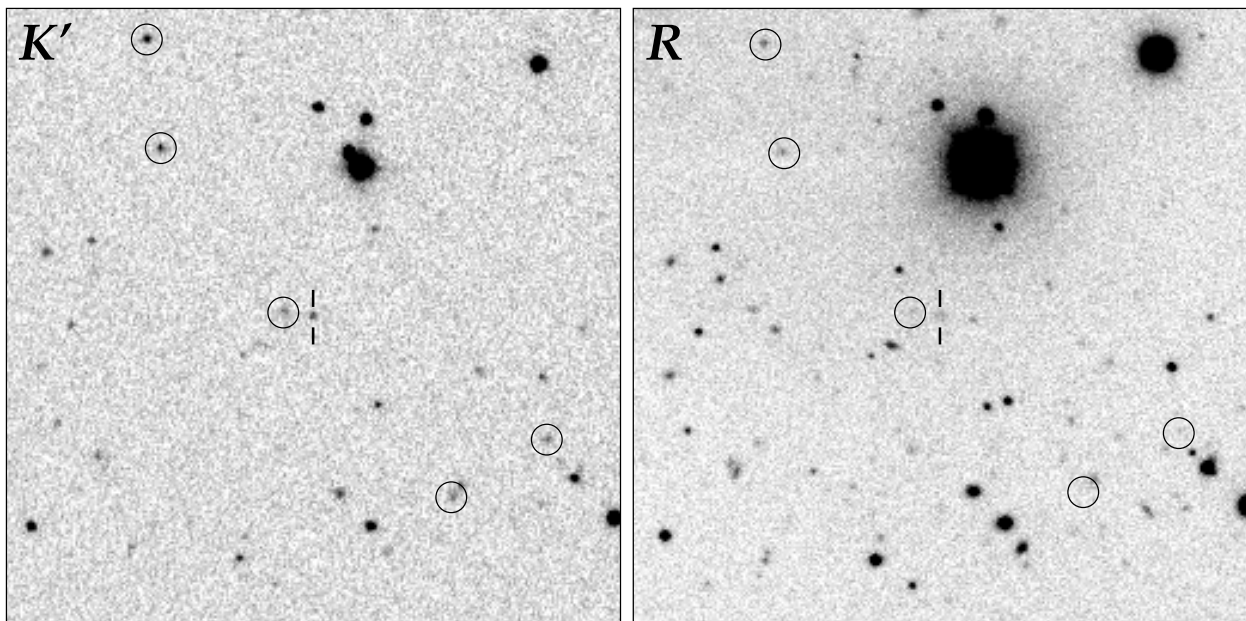


Fig. 1.— Two arcminute square subsections of the K' (left) and R (right) images, centered on B3 0003+387 (tick marks), with north up and east to the left. Several very red galaxies with $(R - K') > 5$ are circled.

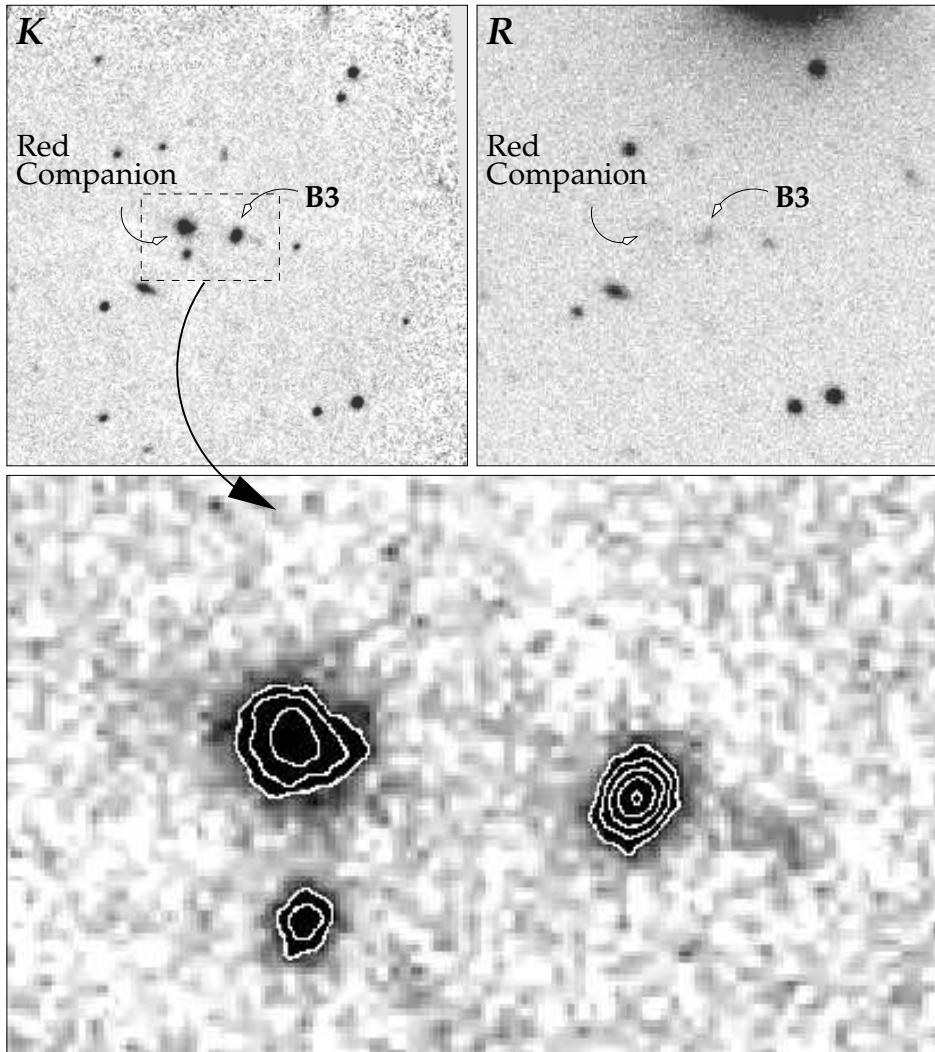


Fig. 2.— Comparison of the Keck K -Band (top left) and WIYN R -band (top right) images in a $40'' \times 40''$ area (1% of the survey area) centered on B3 0003+387. The radio galaxy is identified, as well as the brightest ($K' = 18.36$) and reddest ($(R - K') = 5.^m80$) of several very red objects evident in these images. A $12'' \times 7'.5$ subsection of the K -Band image is also shown (bottom), with contours superimposed. The red companion galaxy is extended in the direction of the radio source, and additional faint features to the west of the radio galaxy and to the east of the red companion are visible in the grayscale image, suggesting that the pair of galaxies may be interacting.

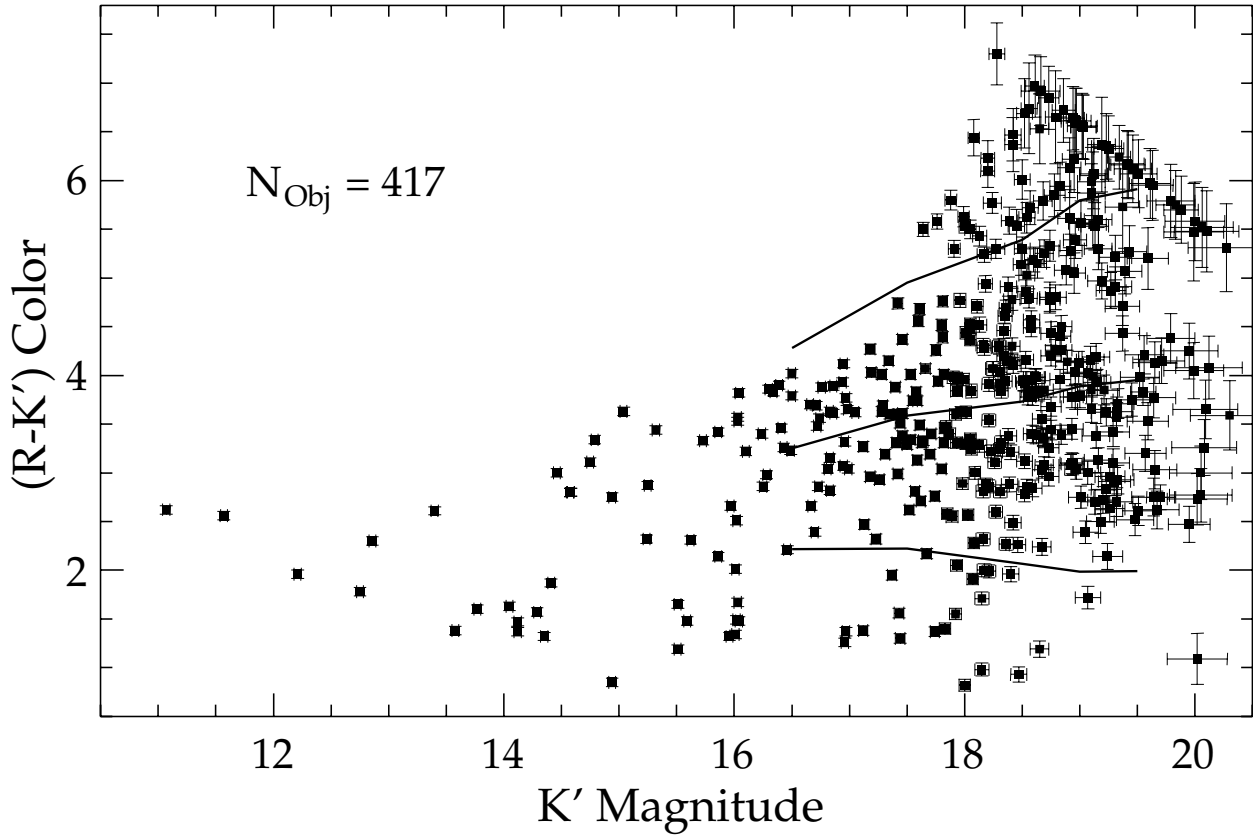


Fig. 3.— The full color-magnitude diagram for objects in the B3 0003+387 field, with error bars showing the $\pm 1\sigma$ uncertainties in both the K' magnitude and $(R - K')$ color. The three solid lines reproduce the median and $\pm 1.75\sigma$ distribution of colors from Thompson et al. (1999).

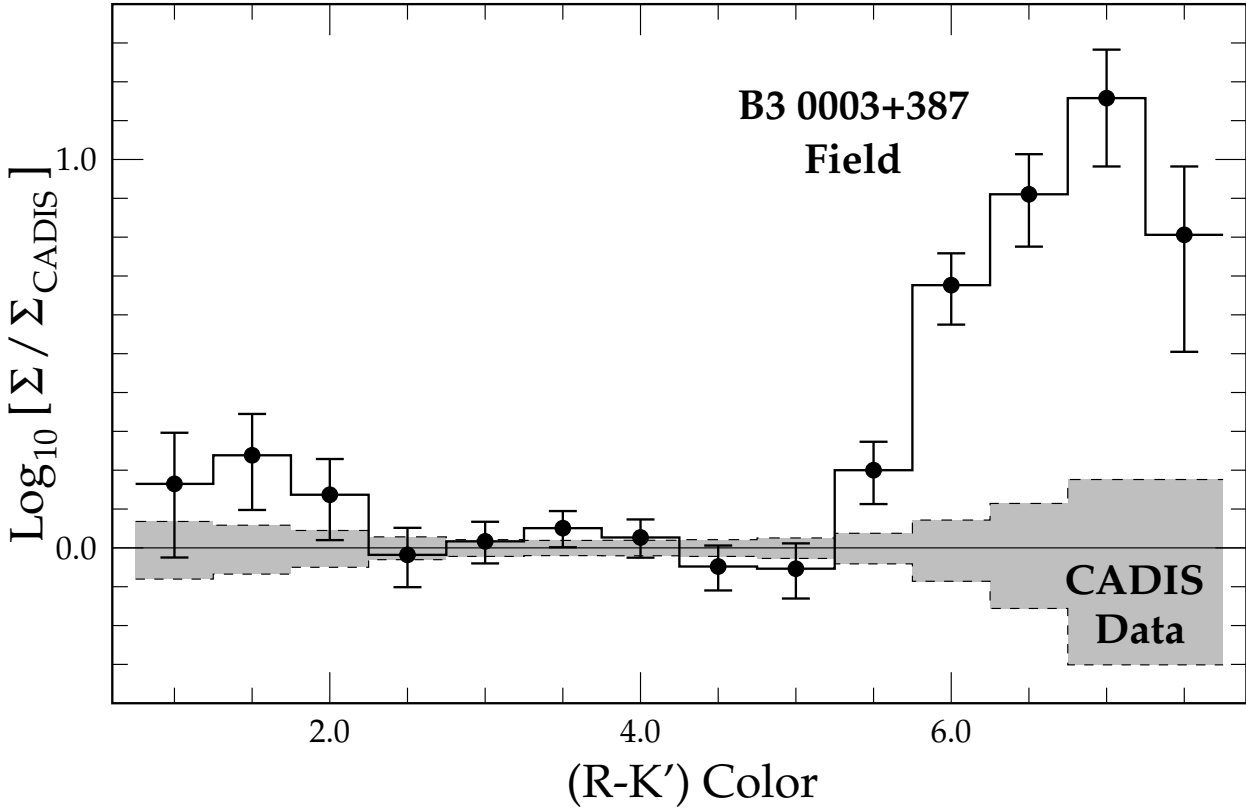


Fig. 4.— The logarithm of the normalized surface density of galaxies in the magnitude range $17.0 \leq K' \leq 19.0$, plotted as a function of the $(R - K')$ color. The data were normalized by an equivalent set of data from CADIS covering over six times the area of the B3 field. The gray region represents the 1σ Poisson uncertainties on the self-normalized CADIS data. Adjacent bins are *not* statistically independent due to the sampling method (see text). A significant overdensity of red galaxies, up to a factor of 14, is evident in the data.

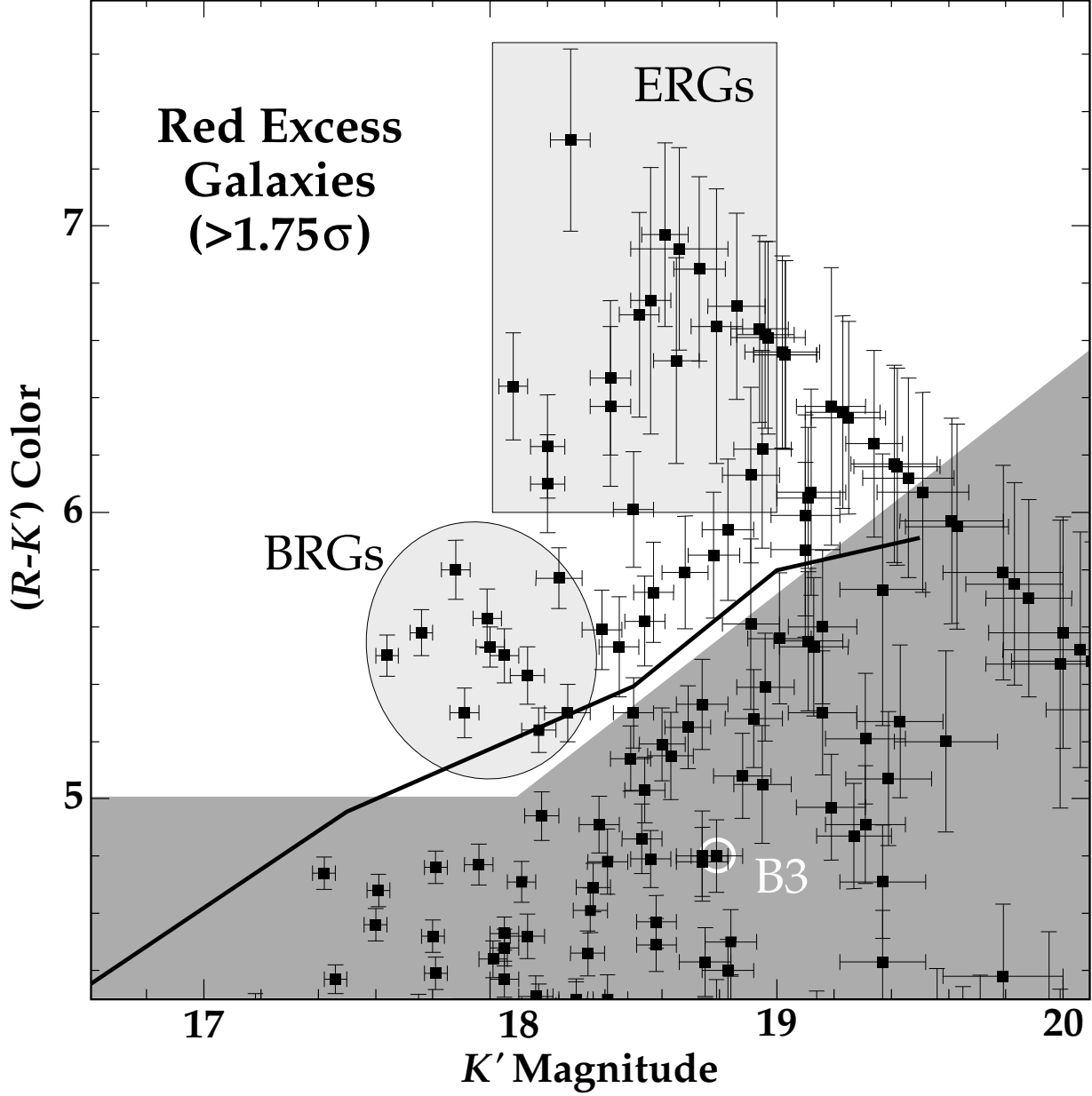


Fig. 5.— Detail from Figure 3. The solid line is the $+1.75\sigma$ line from Thompson et al. (1999). All objects above the dark shaded region ($(R - K') = 0.735K' - 8.23$ for $K' > 18^m$) are the red excess galaxies (REGs). The light shaded oval and rectangle indicate the brightest red galaxies (BRGs) and extremely red galaxies (ERGs), subsets of the REGs. The radio galaxy (B3) is also indicated.

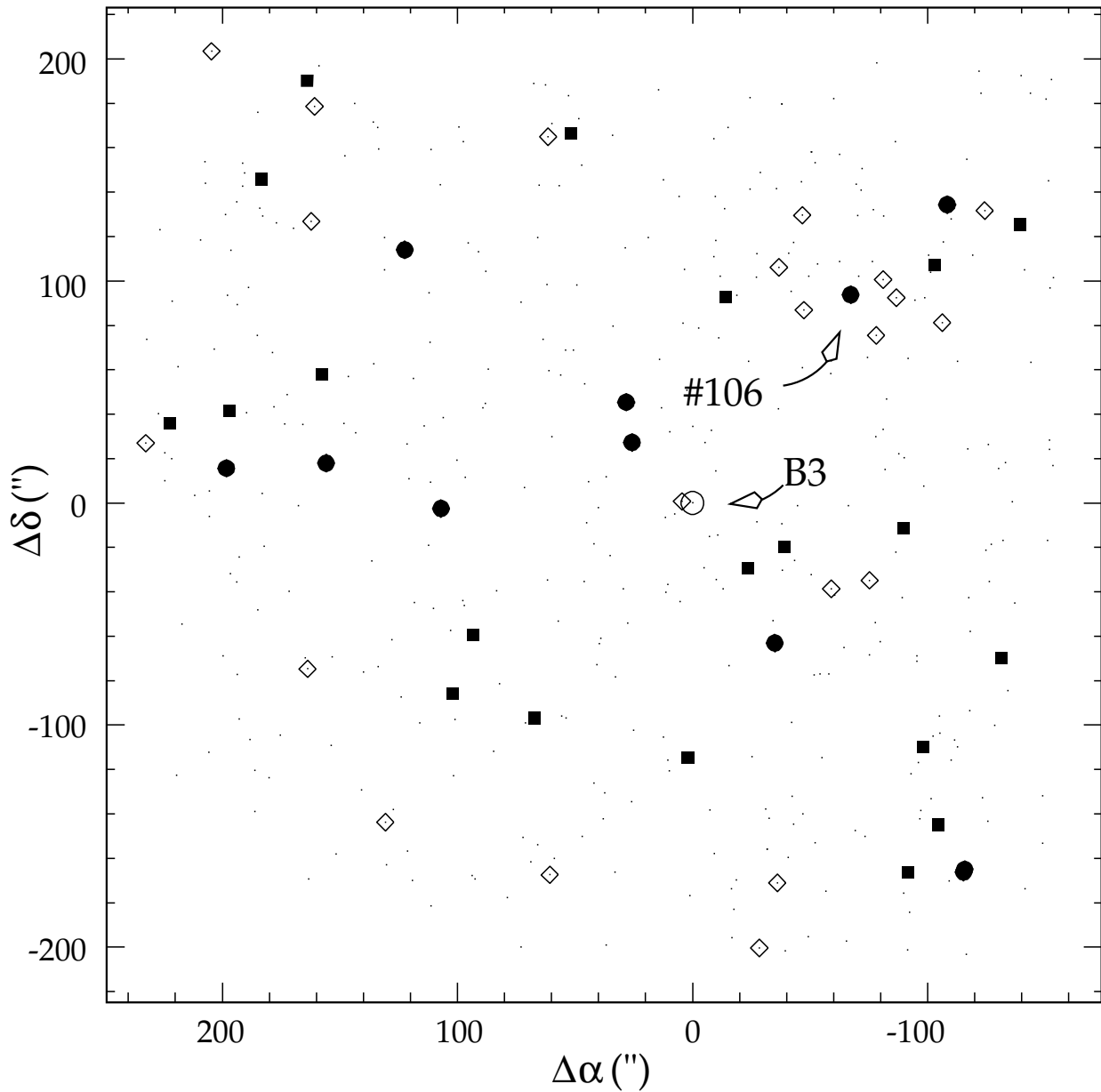


Fig. 6.— The positions of all objects (points) relative to B3 0003+387. Also indicated are the radio galaxy (circled), the BRGs (filled circles), the ERGs (filled squares), and all remaining red objects with $(R - K') > 1.75 \sigma$ (open diamonds).

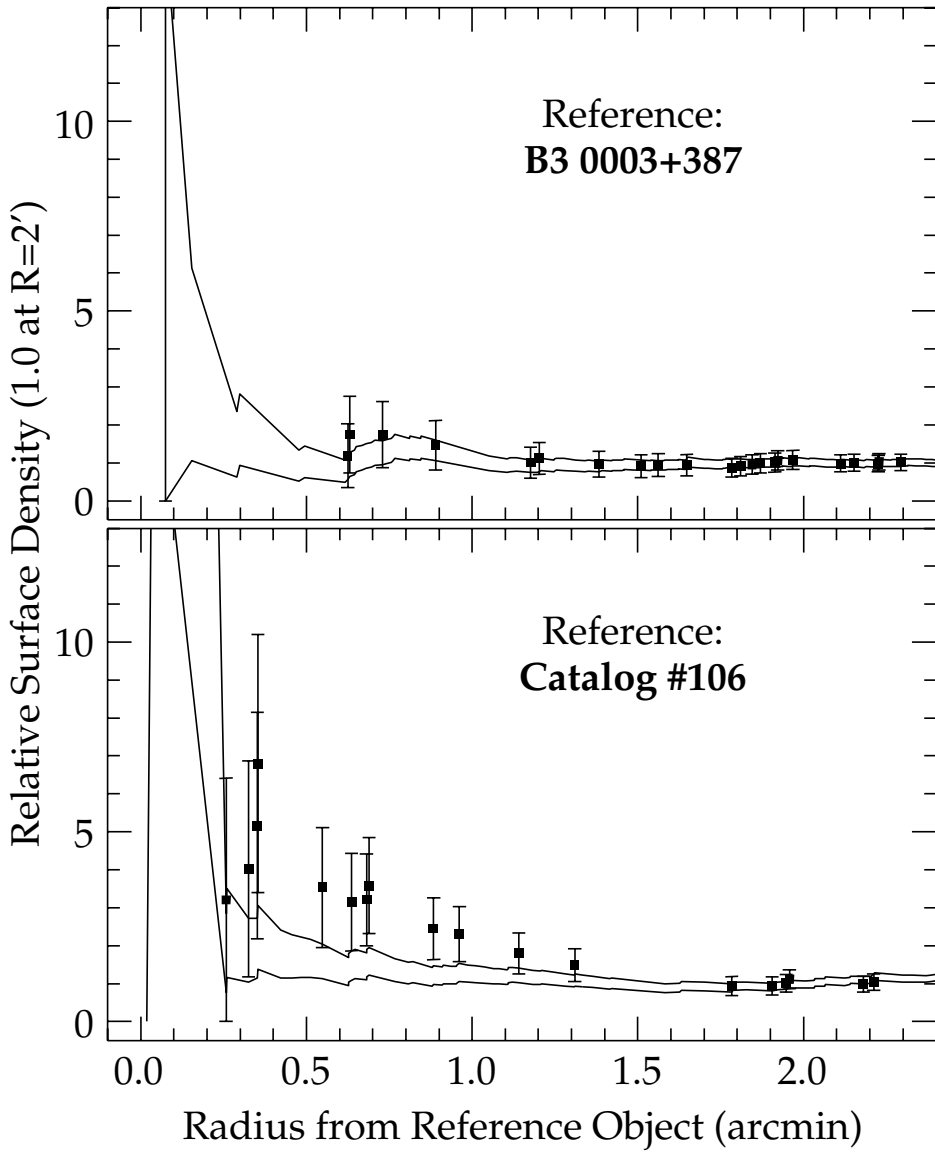


Fig. 7.— The radial surface density of red excess galaxies (filled circles) around B3 0003+387 (top panel) and galaxy #106 (bottom panel). The solid lines plot the $\pm 1\sigma$ surface density of all field objects with $17.0 \leq K' \leq 19.5$, centered on the radio galaxy or #106. The different datasets have been normalized to unity at $r = 2'$.

TABLE 1
PHOTOMETRIC CATALOG^a

$x_{K'}$	$y_{K'}$	K'	$\sigma_{K'}$	x_R	y_R	R	σ_R	α_{J2000}	δ_{J2000}	#
2005.0	1775.7	15.97	0.03	2132.5	1663.5	18.63	0.03	00 06 07.55	+39 02 09.6	1
1997.2	1348.7	19.51	0.14	2140.1	1234.6	22.12	0.05	00 06 07.56	+39 00 44.9	2
2008.1	2226.3	18.93	0.10	2119.4	2115.8	22.03	0.04	00 06 07.62	+39 03 38.9	3
1998.3	1751.7	18.91	0.10	2126.7	1639.2	24.52	0.28	00 06 07.66	+39 02 04.8	4
1990.5	1385.5	19.13	0.12	2132.1	1271.3	21.83	0.04	00 06 07.68	+39 00 52.2	5

^aThe complete version of this table is in the electronic edition of the Journal. The printed edition contains only a sample.

TABLE 2
BRIGHTEST CLUSTER GALAXIES

Cluster ID	z	m_K	Ref
B3 0003+387	1.47?	17.7	1
ClG J0848+4453	1.27	18.1	2
RXJ0848.9+4452	1.26	16.7	3
AXJ2019+112	1.01	17.1	4
Cl 1603+4329	0.92	17.6	5
Cl 1603+4313	0.89	17.0	5

REFERENCES.—(1) This paper, K' ; (2) Stanford et al. (1997), K ; (3) Rosati et al. (1999), K_s ; (4) Benitez et al. (1999), K_s ; (5) Aragón-Salamanca et al. (1993), K .

Table 1. Photometric Catalog

$x_{K'}$	$y_{K'}$	K'	$\sigma_{K'}$	x_R	y_R	R	σ_R	α_{J2000}	δ_{J2000}	#
2005.0	1775.7	15.97	0.03	2132.5	1663.5	18.63	0.03	00 06 07.55	+39 02 09.6	1
1997.2	1348.7	19.51	0.14	2140.1	1234.6	22.12	0.05	00 06 07.56	+39 00 44.9	2
2008.1	2226.3	18.93	0.10	2119.4	2115.8	22.03	0.04	00 06 07.62	+39 03 38.9	3
1998.3	1751.7	18.91	0.10	2126.7	1639.2	24.52	0.28	00 06 07.66	+39 02 04.8	4
1990.5	1385.5	19.13	0.12	2132.1	1271.3	21.83	0.04	00 06 07.68	+39 00 52.2	5
1990.9	1406.4	17.26	0.04	2131.7	1292.4	20.19	0.03	00 06 07.68	+39 00 56.4	6
1998.1	1995.5	18.63	0.08	2117.6	1883.8	23.78	0.13	00 06 07.73	+39 02 53.1	7
1982.7	1178.3	18.95	0.10	2131.8	1063.1	24.00	0.18	00 06 07.76	+39 00 11.1	8
1996.5	2181.3	18.75	0.09	2109.4	2070.3	23.18	0.08	00 06 07.81	+39 03 29.9	9
1961.0	490.5	19.21	0.13	2134.9	371.9	23.06	0.08	00 06 07.93	+38 57 54.8	10
1962.2	598.0	15.04	0.03	2132.2	479.9	18.67	0.03	00 06 07.94	+38 58 16.1	11
1953.8	1583.8	19.55	0.11	2088.1	1469.1	23.38	0.08	00 06 08.37	+39 01 31.4	12
1962.8	2195.4	18.31	0.06	2075.0	2083.3	21.12	0.03	00 06 08.39	+39 03 32.6	13
1921.0	388.0	17.58	0.04	2098.4	267.7	21.41	0.03	00 06 08.58	+38 57 34.3	14
1943.8	1793.7	18.96	0.10	2070.5	1679.4	22.99	0.06	00 06 08.59	+39 02 12.9	15
1944.0	2235.3	17.57	0.04	2054.7	2122.7	20.38	0.03	00 06 08.72	+39 03 40.5	16
1935.4	1897.7	18.56	0.07	2058.2	1783.5	25.30	0.46	00 06 08.77	+39 02 33.5	17
1909.4	1037.8	16.03	0.03	2063.2	919.5	17.70	0.03	00 06 08.96	+38 59 43.1	18
1908.6	1267.7	17.83	0.05	2054.1	1150.2	19.23	0.03	00 06 09.04	+39 00 28.6	19
1892.0	839.0	17.81	0.04	2053.0	719.4	22.20	0.04	00 06 09.20	+38 59 03.6	20
1894.8	1357.2	18.59	0.08	2037.1	1239.5	22.37	0.04	00 06 09.30	+39 00 46.3	21
1886.7	1180.2	18.79	0.09	2035.3	1061.6	23.05	0.06	00 06 09.39	+39 00 11.2	22
1880.4	913.2	18.61	0.08	2038.7	793.4	25.82	0.66	00 06 09.42	+38 59 18.3	23
1880.5	1344.0	17.52	0.04	2023.2	1225.8	20.14	0.03	00 06 09.54	+39 00 43.6	24
1861.8	759.9	19.07	0.11	2025.6	638.9	22.07	0.04	00 06 09.69	+38 58 47.8	25
1876.9	1927.9	19.19	0.12	1998.5	1811.7	24.16	0.14	00 06 09.77	+39 02 39.3	26
1861.8	1171.8	17.92	0.05	2010.7	1052.3	19.47	0.03	00 06 09.81	+39 00 09.5	27
1855.7	1087.6	17.42	0.04	2007.6	967.5	21.02	0.03	00 06 09.89	+38 59 52.8	28
1859.8	1398.1	17.71	0.04	2000.5	1279.4	21.11	0.03	00 06 09.91	+39 00 54.3	29
1844.4	542.6	17.99	0.05	2016.0	420.1	21.95	0.04	00 06 09.93	+38 58 04.7	30
1850.6	1158.6	17.93	0.05	1999.9	1038.7	21.90	0.04	00 06 10.00	+39 00 06.8	31
1860.5	1930.1	19.25	0.13	1981.9	1813.4	26.49	1.00	00 06 10.05	+39 02 39.7	32
1833.2	595.6	15.59	0.03	2002.7	472.9	17.07	0.03	00 06 10.13	+38 58 15.2	33
1857.1	2197.4	19.64	0.19	1968.9	2081.6	23.41	0.08	00 06 10.18	+39 03 32.7	34
1853.4	2247.3	18.53	0.07	1963.4	2131.5	23.39	0.10	00 06 10.26	+39 03 42.5	35
1833.1	1829.0	18.31	0.06	1958.1	1710.9	22.23	0.04	00 06 10.49	+39 02 19.6	36
1814.1	974.2	13.77	0.03	1969.9	852.3	15.37	0.03	00 06 10.57	+38 59 30.2	37
1809.7	794.3	17.74	0.04	1972.0	671.6	20.50	0.03	00 06 10.59	+38 58 54.5	38
1810.8	1051.2	18.21	0.06	1963.8	929.4	22.12	0.04	00 06 10.64	+38 59 45.4	39
1814.7	1389.6	14.79	0.03	1955.5	1269.2	18.13	0.03	00 06 10.67	+39 00 52.5	40
1824.1	2047.7	18.84	0.09	1941.1	1930.1	22.23	0.04	00 06 10.70	+39 03 02.9	41
1790.0	428.0	18.24	0.08	1965.5	304.0	24.01	0.07	00 06 10.82	+38 57 41.9	42
1791.9	240.9	18.84	0.09	1974.2	115.5	23.10	0.08	00 06 10.73	+38 57 04.8	43
1792.1	433.8	18.27	0.08	1967.4	309.1	23.57	0.06	00 06 10.78	+38 57 43.0	44
1782.0	712.0	20.05	0.27	1947.2	588.0	22.82	0.05	00 06 11.04	+38 58 38.1	45
1795.8	1588.1	11.57	0.03	1929.3	1467.8	14.13	0.03	00 06 11.05	+39 01 31.7	46
1775.6	728.7	17.61	0.04	1940.1	604.5	22.29	0.04	00 06 11.15	+38 58 41.4	47
1767.4	682.2	16.49	0.03	1933.6	557.6	19.72	0.03	00 06 11.28	+38 58 32.2	48
1787.8	1912.0	18.93	0.10	1909.7	1792.6	22.38	0.04	00 06 11.28	+39 02 35.9	49

Table 1—Continued

$x_{K'}$	$y_{K'}$	K'	$\sigma_{K'}$	x_R	y_R	R	σ_R	α_{J2000}	δ_{J2000}	#
1758.3	408.5	17.82	0.04	1934.4	282.5	21.83	0.03	00 06 11.35	+38 57 37.9	50
1780.4	1944.8	17.64	0.04	1901.0	1825.3	23.14	0.06	00 06 11.42	+39 02 42.4	51
1770.6	1860.6	17.96	0.05	1894.2	1740.4	22.73	0.05	00 06 11.56	+39 02 25.7	52
1765.0	1677.1	19.03	0.11	1895.2	1556.0	26.49	1.00	00 06 11.60	+39 01 49.3	53
1744.5	744.3	17.42	0.04	1908.4	619.0	22.16	0.04	00 06 11.68	+38 58 44.4	54
1743.4	783.2	17.64	0.04	1905.9	658.1	20.97	0.03	00 06 11.71	+38 58 52.1	55
1736.8	535.5	18.97	0.13	1908.2	409.1	26.49	1.00	00 06 11.75	+38 58 3.0	56
1751.3	1807.8	18.20	0.06	1876.7	1686.8	24.30	0.16	00 06 11.87	+39 02 15.1	57
1729.3	737.5	17.66	0.04	1893.4	611.7	21.73	0.03	00 06 11.94	+38 58 43.0	58
1722.7	595.8	18.58	0.07	1891.9	469.2	23.07	0.06	00 06 12.01	+38 58 14.9	59
1742.1	1791.8	19.59	0.18	1868.1	1670.3	24.79	0.26	00 06 12.02	+39 02 11.9	60
1738.2	1831.0	18.42	0.07	1862.8	1709.5	22.52	0.04	00 06 12.10	+39 02 19.7	61
1728.3	1734.1	14.12	0.03	1856.3	1612.0	15.59	0.03	00 06 12.24	+39 02 00.5	62
1718.8	1306.8	18.67	0.08	1862.2	1182.7	21.70	0.03	00 06 12.28	+39 00 35.7	63
1708.0	713.9	18.73	0.09	1872.9	587.2	26.08	0.80	00 06 12.29	+38 58 38.2	64
1699.9	569.3	18.26	0.06	1870.0	441.8	21.37	0.03	00 06 12.39	+38 58 09.6	65
1698.6	550.1	13.40	0.03	1869.4	422.5	16.01	0.03	00 06 12.41	+38 58 05.8	66
1696.9	678.8	17.28	0.04	1863.0	551.6	21.29	0.03	00 06 12.47	+38 58 31.2	67
1698.1	921.0	16.72	0.03	1855.4	794.7	20.20	0.03	00 06 12.52	+38 59 19.2	68
1697.5	908.9	16.03	0.03	1855.2	782.6	19.60	0.03	00 06 12.53	+38 59 16.8	69
1707.3	1728.7	18.05	0.05	1835.5	1605.8	21.40	0.03	00 06 12.60	+39 01 59.3	70
1681.1	652.8	19.51	0.16	1845.5	523.5	26.49	1.00	00 06 12.73	+38 58 26.0	71
1672.0	338.8	18.17	0.06	1850.3	209.5	20.17	0.03	00 06 12.80	+38 57 23.8	72
1670.8	429.5	18.28	0.07	1845.8	300.5	26.75	1.52	00 06 12.84	+38 57 41.8	73
1690.4	1596.8	18.15	0.06	1823.3	1472.8	19.86	0.03	00 06 12.85	+39 01 33.1	74
1666.1	252.4	17.13	0.04	1847.5	122.6	19.60	0.03	00 06 12.87	+38 57 06.7	75
1678.5	1371.1	18.37	0.06	1819.5	1245.9	22.52	0.04	00 06 12.98	+39 00 48.4	76
1661.0	381.4	15.25	0.03	1837.7	251.8	18.12	0.03	00 06 13.00	+38 57 32.2	77
1674.6	1211.9	18.08	0.05	1821.4	1085.9	24.52	0.18	00 06 13.00	+39 00 16.8	78
1668.5	1053.2	18.52	0.07	1821.0	926.4	21.30	0.03	00 06 13.06	+38 59 45.3	79
1667.1	1380.1	19.99	0.26	1807.7	1254.4	24.04	0.12	00 06 13.18	+39 00 50.1	80
1667.9	1735.3	19.11	0.11	1795.7	1611.0	25.16	0.22	00 06 13.27	+39 02 00.5	81
1656.4	1156.8	18.17	0.06	1805.0	1030.0	22.45	0.04	00 06 13.30	+39 00 05.8	82
1671.7	2089.7	16.41	0.03	1786.7	1966.9	19.87	0.03	00 06 13.31	+39 03 10.7	83
1642.9	1505.8	18.32	0.06	1778.8	1379.8	22.16	0.04	00 06 13.63	+39 01 14.9	84
1637.2	1345.8	18.73	0.09	1778.9	1219.0	21.99	0.04	00 06 13.68	+39 00 43.2	85
1643.4	1921.7	19.65	0.19	1764.3	1797.2	22.68	0.05	00 06 13.74	+39 02 37.3	86
1640.1	1776.8	19.02	0.13	1766.3	1651.6	26.49	1.00	00 06 13.75	+39 02 08.6	87
1634.2	1436.4	17.46	0.04	1772.7	1309.8	21.83	0.03	00 06 13.76	+39 01 01.2	88
1620.0	954.2	19.57	0.18	1775.9	825.3	22.77	0.05	00 06 13.86	+38 59 25.6	89
1635.1	2269.6	18.01	0.05	1743.4	2146.1	21.63	0.04	00 06 13.98	+39 03 46.3	90
1622.7	1650.6	19.46	0.16	1753.4	1524.3	26.49	1.00	00 06 14.01	+39 01 43.6	91
1618.2	1420.0	19.26	0.13	1757.2	1292.8	21.89	0.04	00 06 14.02	+39 00 57.9	92
1610.0	998.0	18.84	0.09	1764.2	868.9	23.34	0.07	00 06 14.04	+38 59 34.2	93
1621.7	1936.1	19.65	0.19	1742.1	1810.9	23.78	0.10	00 06 14.11	+39 02 40.1	94
1617.7	1818.7	19.59	0.18	1742.3	1692.9	23.12	0.06	00 06 14.15	+39 02 16.8	95
1599.2	1094.1	19.12	0.12	1749.9	965.0	25.19	0.34	00 06 14.25	+38 59 53.2	96
1595.8	924.7	16.04	0.03	1752.7	794.9	17.52	0.03	00 06 14.26	+38 59 19.6	97
1603.5	1600.6	17.41	0.04	1735.9	1473.5	20.72	0.03	00 06 14.33	+39 01 33.6	98

Table 1—Continued

$x_{K'}$	$y_{K'}$	K'	$\sigma_{K'}$	x_R	y_R	R	σ_R	α_{J2000}	δ_{J2000}	#
1579.3	512.2	19.32	0.14	1751.0	380.2	22.89	0.05	00 06 14.42	+38 57 57.8	99
1599.7	2030.1	19.37	0.15	1716.5	1904.5	24.08	0.13	00 06 14.52	+39 02 58.7	100
1596.3	1981.3	14.94	0.03	1714.9	1855.4	17.69	0.03	00 06 14.56	+39 02 49.0	101
1587.9	1785.5	20.30	0.34	1713.6	1658.5	23.89	0.11	00 06 14.64	+39 02 10.2	102
1588.3	1923.1	15.32	0.03	1709.0	1796.7	18.76	0.03	00 06 14.68	+39 02 37.4	103
1586.6	1994.9	16.76	0.03	1704.7	1868.7	20.64	0.03	00 06 14.73	+39 02 51.7	104
1558.5	526.4	17.42	0.04	1729.5	393.7	21.02	0.03	00 06 14.78	+38 58 00.6	105
1569.6	1743.5	18.17	0.06	1696.7	1615.8	23.41	0.05	00 06 14.94	+39 02 01.8	106
1567.5	1748.5	18.05	0.05	1694.6	1620.8	22.58	0.03	00 06 14.98	+39 02 02.8	107
1557.0	1264.4	19.31	0.14	1701.3	1134.4	24.52	0.18	00 06 15.02	+39 00 26.8	108
1564.8	1753.0	17.80	0.04	1691.5	1625.1	22.32	0.04	00 06 15.03	+39 02 03.7	109
1535.9	275.3	11.07	0.03	1716.0	140.9	13.69	0.03	00 06 15.09	+38 57 10.8	110
1541.5	942.0	16.73	0.03	1697.5	810.2	19.59	0.03	00 06 15.19	+38 59 22.9	112
1547.7	1819.3	18.59	0.08	1672.0	1691.0	22.54	0.04	00 06 15.34	+39 02 16.7	113
1552.0	2062.6	16.86	0.03	1667.5	1935.4	20.75	0.03	00 06 15.34	+39 03 05.0	114
1524.0	1061.3	19.99	0.26	1675.7	929.4	25.46	0.43	00 06 15.52	+38 59 46.5	115
1540.8	2190.5	17.92	0.05	1651.7	2063.3	21.52	0.03	00 06 15.56	+39 03 30.3	116
1526.1	1594.5	19.33	0.14	1658.4	1464.7	23.04	0.06	00 06 15.64	+39 01 32.1	117
1516.6	1075.9	19.23	0.13	1667.7	943.8	26.49	1.00	00 06 15.65	+38 59 49.3	118
1524.0	1565.5	20.02	0.26	1657.4	1435.5	22.75	0.05	00 06 15.67	+39 01 26.4	119
1508.4	882.8	18.06	0.05	1666.4	749.6	21.30	0.03	00 06 15.73	+38 59 11.0	120
1492.9	389.0	17.40	0.04	1668.7	253.5	21.28	0.03	00 06 15.85	+38 57 33.2	121
1490.4	693.1	18.30	0.06	1655.2	558.7	22.60	0.04	00 06 15.99	+38 58 33.4	122
1489.0	882.7	14.41	0.03	1647.0	748.9	16.28	0.03	00 06 16.06	+38 59 11.0	123
1500.0	1815.0	20.12	0.29	1624.3	1685.0	24.20	0.14	00 06 16.15	+39 02 15.7	124
1472.8	499.2	19.79	0.21	1644.6	363.4	26.49	1.00	00 06 16.23	+38 57 54.9	125
1498.7	2045.2	16.02	0.03	1614.7	1916.1	18.53	0.03	00 06 16.24	+39 03 01.4	126
1476.9	880.6	12.75	0.03	1634.9	746.4	14.53	0.03	00 06 16.27	+38 59 10.5	127
1491.2	2069.8	19.11	0.12	1606.2	1940.5	24.66	0.21	00 06 16.37	+39 03 06.2	128
1473.5	1108.7	14.46	0.03	1623.2	975.2	17.46	0.03	00 06 16.39	+38 59 55.7	130
1480.6	1786.9	20.06	0.27	1605.9	1656.1	25.64	0.51	00 06 16.47	+39 02 10.1	131
1453.8	286.0	18.96	0.10	1633.2	148.8	22.74	0.08	00 06 16.49	+38 57 12.6	132
1468.9	1710.3	19.19	0.12	1596.9	1578.8	25.56	0.47	00 06 16.65	+39 01 54.9	133
1447.3	566.0	17.53	0.04	1616.5	429.5	20.87	0.03	00 06 16.68	+38 58 08.1	134
1463.0	1579.3	17.87	0.05	1595.6	1447.1	21.27	0.03	00 06 16.71	+39 01 28.9	135
1468.8	1925.9	18.78	0.09	1588.9	1795.3	24.63	0.20	00 06 16.71	+39 02 37.6	136
1468.6	2001.5	19.95	0.25	1586.1	1871.2	24.20	0.14	00 06 16.74	+39 02 52.6	137
1446.8	1266.7	18.89	0.10	1590.7	1132.8	23.03	0.06	00 06 16.89	+39 00 26.9	138
1439.8	1141.5	17.23	0.04	1588.2	1006.9	19.55	0.03	00 06 16.98	+39 00 02.1	139
1426.2	542.6	18.36	0.06	1596.2	405.4	20.63	0.03	00 06 17.03	+38 58 03.4	140
1448.8	1864.8	16.83	0.03	1571.1	1733.3	19.98	0.03	00 06 17.03	+39 02 25.5	141
1424.9	605.7	19.15	0.12	1592.7	468.6	23.08	0.06	00 06 17.07	+38 58 15.9	142
1426.5	774.0	20.10	0.28	1588.2	637.6	26.49	1.00	00 06 17.09	+38 58 49.2	143
1442.1	1753.9	19.45	0.16	1568.4	1621.7	23.20	0.06	00 06 17.11	+39 02 03.5	144
1437.8	1840.5	19.70	0.12	1560.9	1708.5	22.45	0.04	00 06 17.21	+39 02 20.6	145
1413.7	466.8	19.61	0.18	1586.4	328.8	26.49	1.00	00 06 17.22	+38 57 48.3	146
1404.5	254.9	18.74	0.09	1584.9	115.8	23.54	0.13	00 06 17.32	+38 57 06.3	147
1417.8	1173.5	18.50	0.07	1565.0	1038.2	24.51	0.19	00 06 17.36	+39 00 08.4	148
1412.3	1119.9	19.16	0.12	1561.4	984.3	24.76	0.24	00 06 17.44	+38 59 57.7	149

Table 1—Continued

$x_{K'}$	$y_{K'}$	K'	$\sigma_{K'}$	x_R	y_R	R	σ_R	α_{J2000}	δ_{J2000}	#
1412.8	1225.8	18.54	0.07	1558.1	1090.5	21.40	0.03	00 06 17.46	+39 00 18.7	150
1429.2	2179.7	18.68	0.08	1540.0	2048.6	22.04	0.04	00 06 17.46	+39 03 27.8	151
1429.3	2179.5	18.68	0.08	1540.1	2048.4	22.05	0.04	00 06 17.46	+39 03 27.7	152
1417.1	1808.1	19.10	0.12	1541.3	1675.2	24.97	0.28	00 06 17.56	+39 02 14.1	153
1410.0	1487.0	14.12	0.03	1545.8	1352.7	15.49	0.03	00 06 17.58	+39 01 10.5	154
1389.3	410.0	19.42	0.15	1564.0	270.9	26.49	1.00	00 06 17.62	+38 57 37.0	155
1414.7	1987.7	19.23	0.13	1532.4	1855.4	22.06	0.04	00 06 17.65	+39 02 49.7	156
1393.3	954.9	17.91	0.05	1548.2	818.0	23.21	0.07	00 06 17.71	+38 59 25.0	157
1391.0	1006.2	18.08	0.05	1544.1	869.4	20.36	0.03	00 06 17.77	+38 59 35.1	158
1374.1	556.8	16.50	0.03	1543.4	417.8	20.52	0.03	00 06 17.92	+38 58 06.0	159
1369.4	486.3	14.58	0.03	1541.3	346.8	17.38	0.03	00 06 17.98	+38 57 52.0	160
1369.4	486.3	14.58	0.03	1541.3	346.8	17.38	0.03	00 06 17.98	+38 57 52.0	161
1367.7	578.1	18.56	0.07	1536.3	438.9	23.35	0.07	00 06 18.04	+38 58 10.2	162
1380.9	2025.1	17.12	0.04	1497.1	1891.7	20.39	0.03	00 06 18.24	+39 02 57.0	163
1348.3	262.6	19.03	0.11	1528.2	121.5	26.49	1.00	00 06 18.27	+38 57 07.7	164
1360.1	1231.4	18.74	0.09	1505.0	1094.3	23.52	0.08	00 06 18.36	+39 00 19.6	165
1370.1	1840.7	16.99	0.03	1493.0	1706.2	20.03	0.03	00 06 18.36	+39 02 20.4	166
1368.4	1787.4	18.31	0.06	1493.2	1652.7	21.55	0.03	00 06 18.38	+39 02 09.8	167
1339.5	697.1	17.85	0.05	1503.6	557.3	20.43	0.03	00 06 18.55	+38 58 33.7	168
1344.8	1135.1	18.11	0.05	1493.1	997.2	22.82	0.05	00 06 18.59	+39 00 00.5	169
1358.4	1987.0	18.25	0.06	1475.9	1852.7	22.32	0.04	00 06 18.61	+39 02 49.4	170
1361.8	2195.2	18.74	0.09	1471.9	2061.8	24.07	0.13	00 06 18.61	+39 03 30.6	171
1348.3	1595.5	17.37	0.04	1480.0	1459.4	19.32	0.03	00 06 18.66	+39 01 31.8	172
1338.4	1125.0	18.42	0.07	1487.0	986.7	24.89	0.26	00 06 18.69	+38 59 58.5	173
1325.3	1746.9	18.52	0.07	1451.4	1610.5	22.44	0.04	00 06 19.10	+39 02 01.7	174
1301.1	418.0	17.29	0.04	1475.2	275.8	20.98	0.03	00 06 19.12	+38 57 38.3	175
1294.4	351.0	18.39	0.07	1470.9	208.4	21.27	0.03	00 06 19.21	+38 57 25.0	176
1290.1	286.8	19.63	0.18	1468.9	143.7	26.49	1.00	00 06 19.27	+38 57 12.2	177
1290.5	398.2	16.04	0.03	1465.3	255.5	19.86	0.03	00 06 19.29	+38 57 34.3	178
1294.3	905.3	17.55	0.04	1450.7	764.7	21.29	0.03	00 06 19.38	+38 59 14.8	179
1313.8	2127.9	16.71	0.03	1426.1	1992.5	20.40	0.03	00 06 19.41	+39 03 17.1	180
1302.5	1742.4	18.52	0.07	1428.7	1605.2	25.21	0.35	00 06 19.49	+39 02 00.7	181
1302.9	1943.8	13.58	0.03	1421.8	1807.4	14.96	0.03	00 06 19.54	+39 02 40.6	182
1284.6	1080.1	19.24	0.13	1434.6	939.8	21.38	0.03	00 06 19.60	+38 59 49.4	183
1289.8	1790.8	17.44	0.04	1414.2	1653.3	18.74	0.03	00 06 19.71	+39 02 10.3	184
1285.1	1650.6	19.07	0.11	1414.5	1512.4	20.79	0.03	00 06 19.75	+39 01 42.5	185
1275.5	1202.7	18.21	0.06	1421.1	1062.5	21.75	0.03	00 06 19.79	+39 00 13.7	186
1269.9	1101.3	16.95	0.03	1419.1	960.6	20.02	0.03	00 06 19.85	+38 59 53.6	187
1282.8	1872.2	19.71	0.20	1404.2	1734.7	23.86	0.12	00 06 19.86	+39 02 26.4	188
1272.9	1348.3	18.59	0.08	1413.3	1208.6	21.43	0.03	00 06 19.87	+39 00 42.5	189
1283.4	1971.8	19.20	0.13	1401.2	1834.8	21.92	0.04	00 06 19.88	+39 02 46.1	190
1255.8	478.4	18.52	0.07	1427.5	334.9	21.64	0.03	00 06 19.91	+38 57 50.1	191
1278.0	1835.6	17.67	0.04	1400.7	1697.8	19.84	0.03	00 06 19.93	+39 02 19.1	192
1282.1	2103.5	18.34	0.06	1395.2	1966.9	22.80	0.05	00 06 19.94	+39 03 12.2	193
1266.1	1440.5	15.86	0.03	1403.1	1300.9	19.28	0.03	00 06 20.02	+39 01 00.8	194
1247.3	578.4	17.89	0.05	1415.4	434.9	20.44	0.03	00 06 20.08	+38 58 09.9	195
1257.3	1198.9	19.95	0.18	1403.0	1058.1	22.42	0.04	00 06 20.09	+39 00 12.9	196
1251.8	1412.8	14.94	0.03	1389.7	1272.6	15.79	0.03	00 06 20.25	+39 00 55.2	197
1244.6	1128.0	17.82	0.04	1392.8	986.5	21.13	0.03	00 06 20.29	+38 59 58.8	198

Table 1—Continued

$x_{K'}$	$y_{K'}$	K'	$\sigma_{K'}$	x_R	y_R	R	σ_R	α_{J2000}	δ_{J2000}	#
1242.4	1673.3	18.96	0.10	1370.8	1533.7	24.35	0.16	00 06 20.49	+39 01 46.8	199
1226.3	1450.3	16.86	0.03	1362.7	1309.3	20.47	0.03	00 06 20.70	+39 01 02.6	200
1222.2	1276.2	18.79	0.09	1364.9	1134.4	23.59	0.09	00 06 20.71	+39 00 28.1	201
1201.0	384.5	18.67	0.08	1375.9	238.7	20.91	0.03	00 06 20.81	+38 57 31.3	202
1214.8	697.1	18.94	0.10	1378.1	552.6	25.66	0.67	00 06 20.88	+38 58 33.3	203
1215.0	1532.4	18.73	0.09	1348.5	1391.3	21.69	0.03	00 06 20.91	+39 01 18.8	204
1213.9	1806.9	16.43	0.03	1337.4	1666.8	19.69	0.03	00 06 21.01	+39 02 13.2	205
1209.3	1685.0	17.93	0.05	1337.2	1544.2	21.77	0.03	00 06 21.05	+39 01 49.0	206
1200.1	1280.0	18.54	0.07	1342.6	1137.4	24.16	0.14	00 06 21.09	+39 00 28.7	207
1191.8	1052.4	19.64	0.19	1342.5	908.7	22.39	0.04	00 06 21.16	+38 59 43.6	208
1206.0	1973.1	18.93	0.10	1323.5	1833.3	22.71	0.05	00 06 21.20	+39 02 46.1	209
1182.9	1251.6	19.16	0.12	1326.4	1108.4	22.29	0.04	00 06 21.37	+39 00 23.1	210
1176.2	1438.9	20.09	0.28	1312.9	1296.1	23.74	0.11	00 06 21.54	+39 01 00.2	211
1161.7	668.1	18.69	0.08	1326.2	521.9	21.77	0.03	00 06 21.56	+38 58 27.4	212
1159.3	692.7	16.28	0.03	1322.9	546.5	19.26	0.03	00 06 21.61	+38 58 32.2	213
1166.1	1092.1	19.52	0.17	1315.3	947.6	23.50	0.08	00 06 21.61	+38 59 51.4	214
1161.0	1074.5	18.16	0.06	1310.9	929.8	20.48	0.03	00 06 21.69	+38 59 47.9	215
1163.8	1244.3	20.08	0.28	1307.5	1100.3	23.34	0.07	00 06 21.70	+39 00 21.6	216
1150.3	745.6	18.88	0.10	1312.0	599.3	23.96	0.11	00 06 21.78	+38 58 42.7	217
1172.5	2011.7	19.10	0.12	1288.4	1870.9	22.95	0.07	00 06 21.78	+39 02 53.6	218
1159.7	1493.8	20.05	0.27	1294.4	1350.6	23.05	0.06	00 06 21.84	+39 01 11.0	219
1157.3	1603.5	15.24	0.03	1287.9	1460.6	17.56	0.03	00 06 21.91	+39 01 32.7	220
1165.5	2216.7	15.51	0.03	1274.0	2076.4	17.16	0.03	00 06 21.96	+39 03 34.2	221
1138.0	1881.0	18.51	0.07	1258.5	1738.5	22.45	0.07	00 06 22.32	+39 02 27.6	222
1087.1	761.7	17.18	0.04	1248.0	613.2	20.14	0.03	00 06 22.86	+38 58 45.7	223
1095.0	1415.8	18.00	0.05	1232.2	1270.0	23.53	0.05	00 06 22.92	+39 00 55.3	224
1079.3	599.1	18.35	0.06	1246.0	449.7	22.29	0.04	00 06 22.94	+38 58 13.4	225
1078.0	1005.2	19.83	0.17	1230.0	857.3	26.27	0.91	00 06 23.08	+38 59 33.9	226
1084.1	1507.4	17.76	0.04	1218.0	1361.5	23.34	0.07	00 06 23.13	+39 01 13.4	227
1088.5	1858.8	18.09	0.05	1209.8	1714.4	21.09	0.04	00 06 23.16	+39 02 23.1	228
1070.0	1083.7	19.23	0.13	1219.2	935.8	22.85	0.05	00 06 23.24	+38 59 49.4	229
1050.0	883.1	14.35	0.03	1206.4	733.8	15.67	0.03	00 06 23.52	+38 59 09.6	230
1041.5	439.5	19.33	0.14	1213.9	288.2	22.26	0.04	00 06 23.54	+38 57 41.7	231
1058.5	1680.9	19.07	0.11	1186.0	1534.8	23.09	0.06	00 06 23.62	+39 01 47.7	232
1065.5	2114.1	18.59	0.08	1177.4	1969.8	21.99	0.04	00 06 23.63	+39 03 13.6	233
1043.2	1159.5	18.31	0.06	1189.5	1011.0	22.34	0.04	00 06 23.72	+39 00 04.4	234
1019.0	274.5	19.37	0.15	1197.3	121.8	25.10	0.45	00 06 23.87	+38 57 08.9	235
1037.9	1338.6	18.75	0.09	1177.7	1190.5	22.19	0.04	00 06 23.87	+39 00 39.8	236
1021.8	621.0	18.67	0.08	1187.5	469.6	22.22	0.04	00 06 23.92	+38 58 17.6	237
1018.4	561.9	18.13	0.06	1186.2	410.2	21.41	0.03	00 06 23.97	+38 58 05.9	238
1020.5	971.5	19.48	0.16	1173.5	821.4	22.00	0.04	00 06 24.05	+38 59 27.0	239
1016.9	959.9	17.93	0.05	1170.4	809.6	19.98	0.03	00 06 24.11	+38 59 24.7	240
1020.2	1269.3	19.29	0.14	1162.5	1120.3	22.39	0.04	00 06 24.14	+39 00 26.0	241
1010.5	911.7	20.00	0.26	1165.7	761.1	26.49	1.00	00 06 24.20	+38 59 15.2	242
1000.3	643.5	18.69	0.08	1165.1	491.5	23.94	0.12	00 06 24.30	+38 58 22.0	243
1009.4	1187.0	19.32	0.14	1154.5	1037.3	22.95	0.05	00 06 24.30	+39 00 09.7	244
999.6	1328.8	18.16	0.06	1139.7	1179.3	22.47	0.04	00 06 24.51	+39 00 37.7	248
994.2	1234.9	19.14	0.12	1137.6	1084.8	22.52	0.04	00 06 24.58	+39 00 19.1	249
995.9	1551.1	15.86	0.03	1127.9	1402.3	18.00	0.03	00 06 24.64	+39 01 21.8	250

Table 1—Continued

$x_{K'}$	$y_{K'}$	K'	$\sigma_{K'}$	x_R	y_R	R	σ_R	α_{J2000}	δ_{J2000}	#
987.0	1101.1	16.97	0.03	1135.2	950.4	20.74	0.03	00 06 24.66	+38 59 52.6	251
972.9	522.5	12.21	0.03	1142.0	369.1	14.17	0.03	00 06 24.73	+38 57 57.9	252
998.0	2047.5	17.84	0.05	1112.0	1900.6	21.31	0.04	00 06 24.75	+39 03 00.2	253
993.1	2153.6	17.93	0.05	1103.3	2006.9	21.24	0.03	00 06 24.87	+39 03 21.2	254
982.1	1775.2	18.41	0.07	1106.0	1626.7	23.19	0.09	00 06 24.94	+39 02 06.1	255
973.4	1627.8	18.34	0.06	1102.5	1478.5	22.54	0.04	00 06 25.05	+39 01 36.9	256
975.7	2121.3	18.96	0.10	1087.0	1973.9	25.79	0.81	00 06 25.16	+39 03 14.7	257
972.6	2205.8	17.70	0.04	1080.8	2058.6	20.89	0.03	00 06 25.23	+39 03 31.4	258
942.3	791.9	16.95	0.03	1101.5	638.4	21.07	0.03	00 06 25.33	+38 58 51.2	259
955.4	1627.9	17.53	0.04	1084.5	1478.0	21.54	0.03	00 06 25.35	+39 01 36.9	260
932.5	796.4	16.83	0.03	1091.5	642.5	20.46	0.03	00 06 25.49	+38 58 52.0	261
944.9	1571.9	18.21	0.06	1076.0	1421.4	21.07	0.03	00 06 25.52	+39 01 25.7	262
949.2	2002.0	17.42	0.04	1064.7	1853.2	20.41	0.03	00 06 25.57	+39 02 51.0	263
928.6	1011.9	16.96	0.03	1079.9	858.7	20.28	0.03	00 06 25.62	+38 59 34.7	264
911.9	472.9	18.69	0.08	1082.6	317.2	22.54	0.05	00 06 25.75	+38 57 47.9	265
923.3	1432.2	19.18	0.12	1059.3	1280.4	21.68	0.03	00 06 25.84	+39 00 58.0	266
936.0	2142.8	18.41	0.07	1046.3	1994.1	22.71	0.05	00 06 25.84	+39 03 18.8	267
901.0	436.3	19.10	0.12	1073.0	280.0	25.09	0.33	00 06 25.92	+38 57 40.6	268
919.1	1581.6	19.29	0.14	1049.7	1430.2	22.71	0.05	00 06 25.96	+39 01 27.6	269
927.4	2113.4	19.34	0.10	1038.8	1964.3	26.91	2.10	00 06 25.98	+39 03 13.0	270
908.3	1106.0	19.67	0.19	1056.1	952.5	22.29	0.04	00 06 26.00	+38 59 53.3	271
918.8	1778.0	18.32	0.06	1042.3	1627.3	21.63	0.04	00 06 26.02	+39 02 06.5	272
923.9	2231.3	16.98	0.03	1031.1	2082.5	20.63	0.03	00 06 26.07	+39 03 36.3	273
907.6	1653.3	18.75	0.09	1035.6	1501.7	22.43	0.04	00 06 26.17	+39 01 41.7	274
906.0	2004.0	18.16	0.06	1021.3	1853.7	20.97	0.03	00 06 26.31	+39 02 51.2	275
875.7	504.8	16.01	0.03	1045.1	347.9	18.02	0.03	00 06 26.37	+38 57 54.1	276
900.1	1884.7	18.06	0.05	1019.7	1733.8	21.90	0.05	00 06 26.37	+39 02 27.6	277
874.8	792.0	18.86	0.10	1033.8	636.1	26.25	0.89	00 06 26.47	+38 58 51.0	278
898.0	2234.8	18.36	0.06	1004.9	2085.1	23.05	0.06	00 06 26.51	+39 03 36.9	279
861.0	465.9	18.18	0.06	1031.7	308.3	21.06	0.03	00 06 26.61	+38 57 46.3	280
855.0	782.4	19.11	0.12	1014.3	625.8	23.10	0.06	00 06 26.81	+38 58 49.0	281
862.8	1317.3	18.58	0.07	1002.7	1162.9	23.15	0.06	00 06 26.84	+39 00 35.0	282
845.3	522.1	19.32	0.14	1013.9	364.2	22.02	0.04	00 06 26.89	+38 57 57.4	283
836.9	272.8	18.27	0.06	1014.6	113.6	20.87	0.03	00 06 26.96	+38 57 08.0	284
862.1	1738.7	20.27	0.33	986.8	1585.8	28.65	8.72	00 06 26.97	+39 01 58.5	285
809.0	385.6	18.21	0.06	982.5	225.8	20.20	0.03	00 06 27.47	+38 57 30.2	286
800.2	872.2	18.40	0.07	956.1	713.9	21.61	0.03	00 06 27.76	+38 59 06.6	287
797.8	1083.1	18.94	0.10	946.0	925.5	22.03	0.04	00 06 27.87	+38 59 48.4	288
785.4	718.7	19.30	0.14	946.7	559.4	22.21	0.04	00 06 27.97	+38 58 36.2	289
788.9	1586.9	17.50	0.04	918.9	1430.9	20.79	0.03	00 06 28.17	+39 01 28.2	290
788.4	1809.7	18.53	0.07	910.3	1654.5	22.69	0.05	00 06 28.25	+39 02 12.3	291
781.9	1510.0	17.97	0.05	914.6	1353.5	21.59	0.03	00 06 28.27	+39 01 12.9	292
775.5	1499.4	18.62	0.08	908.6	1342.6	22.01	0.04	00 06 28.37	+39 01 10.8	293
773.0	1855.2	16.46	0.03	893.1	1699.6	18.67	0.03	00 06 28.52	+39 02 21.3	294
740.9	429.8	16.74	0.03	912.5	267.8	20.30	0.03	00 06 28.64	+38 57 38.8	295
746.8	983.5	18.20	0.06	898.4	823.8	24.43	0.17	00 06 28.71	+38 59 28.5	296
734.5	437.9	17.28	0.04	905.8	275.7	20.91	0.03	00 06 28.75	+38 57 40.3	297
751.7	1874.8	16.24	0.03	871.1	1718.6	19.64	0.03	00 06 28.89	+39 02 25.1	298
735.9	1343.2	18.64	0.08	874.5	1184.4	22.47	0.04	00 06 29.00	+39 00 39.7	299

Table 1—Continued

$x_{K'}$	$y_{K'}$	K'	$\sigma_{K'}$	x_R	y_R	R	σ_R	α_{J2000}	δ_{J2000}	#
728.2	1051.1	17.61	0.04	877.3	891.0	21.10	0.03	00 06 29.04	+38 59 41.8	300
745.5	2105.0	17.19	0.04	856.6	1949.4	21.22	0.03	00 06 29.07	+39 03 10.7	301
725.7	1062.0	18.05	0.05	874.4	901.8	22.53	0.04	00 06 29.09	+38 59 44.0	302
736.1	2139.1	20.02	0.26	845.9	1983.3	21.11	0.03	00 06 29.24	+39 03 17.4	303
718.5	1381.6	18.41	0.07	855.6	1222.3	22.56	0.04	00 06 29.31	+39 00 47.3	304
704.0	792.9	18.55	0.07	862.4	631.0	22.33	0.04	00 06 29.38	+38 58 50.6	305
697.9	665.0	15.62	0.03	860.9	502.4	17.93	0.03	00 06 29.44	+38 58 25.2	306
699.0	851.6	18.95	0.10	855.2	689.7	25.17	0.33	00 06 29.48	+38 59 02.2	307
698.2	995.4	19.39	0.15	849.2	834.0	24.46	0.18	00 06 29.54	+38 59 30.7	308
690.5	1479.3	17.46	0.04	823.9	1319.5	21.07	0.03	00 06 29.81	+39 01 06.5	309
682.5	1272.6	17.99	0.05	823.5	1111.7	23.62	0.09	00 06 29.89	+39 00 25.6	310
694.4	2007.8	17.75	0.04	808.8	1850.0	22.01	0.04	00 06 29.91	+39 02 51.3	311
661.9	1045.7	16.01	0.03	810.9	883.2	17.35	0.03	00 06 30.17	+38 59 40.5	312
644.9	370.3	18.83	0.09	818.4	204.7	22.79	0.05	00 06 30.25	+38 57 26.6	313
675.1	2088.5	19.27	0.13	786.5	1930.4	24.14	0.13	00 06 30.26	+39 03 07.2	314
660.4	1333.0	19.09	0.12	799.0	1171.5	23.25	0.07	00 06 30.28	+39 00 37.4	315
665.3	1650.8	17.77	0.04	792.5	1490.6	21.71	0.03	00 06 30.29	+39 01 40.4	316
665.1	1762.7	19.88	0.15	788.2	1602.9	27.40	2.52	00 06 30.33	+39 02 02.6	317
654.0	1189.9	18.60	0.08	797.8	1027.7	23.79	0.10	00 06 30.35	+39 00 09.1	318
650.0	1461.0	19.14	0.12	784.0	1299.6	23.33	0.07	00 06 30.50	+39 01 02.8	319
628.4	786.0	15.73	0.03	786.7	621.3	19.06	0.03	00 06 30.66	+38 58 49.0	320
621.5	1059.5	16.70	0.03	769.9	895.6	19.09	0.03	00 06 30.86	+38 59 43.1	321
628.5	1568.8	18.24	0.06	758.5	1407.1	22.31	0.04	00 06 30.89	+39 01 24.1	322
605.5	428.2	19.05	0.11	776.7	261.4	21.44	0.03	00 06 30.94	+38 57 38.0	323
614.9	1341.1	18.97	0.10	753.1	1178.0	22.01	0.04	00 06 31.06	+39 00 38.9	324
596.5	494.9	18.38	0.07	765.2	328.0	23.29	0.07	00 06 31.11	+38 57 51.2	325
612.6	1420.7	18.03	0.05	747.9	1257.8	20.60	0.03	00 06 31.12	+39 00 54.7	326
615.4	1861.6	18.13	0.06	734.8	1700.5	23.56	0.08	00 06 31.21	+39 02 22.0	327
589.0	846.3	19.01	0.11	745.0	680.5	24.57	0.20	00 06 31.35	+38 59 00.8	328
568.3	590.3	19.26	0.13	733.4	422.8	22.22	0.04	00 06 31.62	+38 58 10.0	329
571.3	976.1	15.96	0.03	722.5	810.2	17.28	0.03	00 06 31.69	+38 59 26.4	330
551.1	465.6	18.75	0.09	720.8	297.0	22.95	0.05	00 06 31.87	+38 57 45.2	331
550.2	561.9	18.83	0.09	716.4	393.7	24.77	0.23	00 06 31.92	+38 58 04.3	332
570.7	1817.2	17.59	0.04	691.5	1654.3	21.33	0.03	00 06 31.95	+39 02 13.1	333
572.1	1890.5	17.35	0.04	690.2	1728.0	20.95	0.03	00 06 31.95	+39 02 27.6	334
563.5	2092.2	18.62	0.08	674.4	1930.1	22.60	0.04	00 06 32.16	+39 03 07.6	335
541.0	916.0	14.05	0.03	694.3	748.7	15.68	0.03	00 06 32.18	+38 59 14.4	336
562.1	2140.3	19.56	0.17	671.2	1978.3	23.77	0.10	00 06 32.20	+39 03 17.1	337
544.1	1603.7	17.46	0.04	672.6	1439.1	20.84	0.03	00 06 32.34	+39 01 30.7	338
552.6	2152.7	18.46	0.07	661.3	1990.5	20.72	0.03	00 06 32.36	+39 03 19.5	339
531.9	1155.8	17.62	0.04	676.5	989.1	20.33	0.03	00 06 32.41	+39 00 01.9	340
509.9	904.2	16.34	0.03	663.5	735.7	20.17	0.03	00 06 32.71	+38 59 12.0	341
500.2	636.3	16.30	0.03	663.5	466.5	20.16	0.03	00 06 32.79	+38 58 18.9	342
501.7	1448.2	17.60	0.04	635.6	1281.5	22.16	0.04	00 06 33.01	+39 00 59.7	343
513.9	2195.9	17.63	0.04	620.8	2032.4	20.94	0.03	00 06 33.03	+39 03 27.9	344
488.9	1575.9	12.86	0.03	618.1	1409.2	15.16	0.03	00 06 33.27	+39 01 25.0	345
490.7	2077.8	19.10	0.12	601.8	1913.1	22.75	0.05	00 06 33.39	+39 03 04.5	346
477.4	1469.2	18.05	0.05	610.5	1301.7	21.38	0.03	00 06 33.43	+39 01 03.8	347
443.2	491.3	19.01	0.11	611.5	319.0	21.76	0.03	00 06 33.72	+38 57 49.9	348

Table 1—Continued

$x_{K'}$	$y_{K'}$	K'	$\sigma_{K'}$	x_R	y_R	R	σ_R	α_{J2000}	δ_{J2000}	#
442.8	939.4	16.67	0.03	594.9	768.8	19.33	0.03	00 06 33.86	+38 59 18.7	349
437.2	738.3	17.44	0.04	596.5	566.7	20.95	0.03	00 06 33.89	+38 58 38.9	350
437.9	1379.9	17.88	0.05	574.0	1210.7	23.68	0.09	00 06 34.08	+39 00 46.0	351
432.3	1581.9	18.42	0.07	561.1	1413.3	24.79	0.27	00 06 34.23	+39 01 26.0	352
437.9	2283.4	18.13	0.06	541.4	2117.6	22.65	0.05	00 06 34.35	+39 03 45.0	353
427.4	2190.8	19.41	0.15	534.1	2024.3	26.20	0.88	00 06 34.50	+39 03 26.6	354
415.6	1929.6	18.39	0.07	531.7	1761.7	23.98	0.12	00 06 34.62	+39 02 34.8	355
382.9	435.2	16.97	0.03	553.0	260.5	18.34	0.03	00 06 34.72	+38 57 38.6	356
389.2	913.2	18.68	0.08	542.1	740.6	24.47	0.18	00 06 34.76	+38 59 13.4	357
412.9	2249.7	18.79	0.09	517.5	2082.9	25.44	0.47	00 06 34.77	+39 03 38.2	358
384.6	938.5	17.18	0.04	536.5	765.8	21.45	0.03	00 06 34.85	+38 59 18.3	359
388.4	1469.1	19.16	0.12	521.2	1298.5	24.46	0.18	00 06 34.94	+39 01 03.5	360
376.4	1284.4	18.01	0.05	515.8	1112.7	21.31	0.03	00 06 35.09	+39 00 26.9	361
377.4	1914.5	18.54	0.07	494.0	1745.1	23.57	0.09	00 06 35.27	+39 02 31.7	362
352.8	1089.7	14.75	0.03	499.1	916.4	17.86	0.03	00 06 35.43	+38 59 48.2	363
356.6	1536.7	16.96	0.03	486.8	1365.1	18.22	0.03	00 06 35.51	+39 01 16.8	364
350.2	1470.8	19.43	0.15	482.8	1298.9	24.70	0.22	00 06 35.59	+39 01 03.7	365
328.3	763.7	18.18	0.06	486.3	588.4	23.12	0.06	00 06 35.75	+38 58 43.5	366
341.3	1927.3	18.23	0.06	457.3	1756.7	21.45	0.03	00 06 35.89	+39 02 34.1	367
327.8	1509.7	18.61	0.08	458.9	1337.1	22.59	0.04	00 06 35.99	+39 01 11.3	368
327.6	1633.2	18.42	0.07	454.2	1461.0	20.91	0.03	00 06 36.03	+39 01 35.8	369
302.3	667.1	16.66	0.03	463.7	490.4	20.36	0.03	00 06 36.16	+38 58 24.3	370
301.6	1193.5	17.83	0.05	443.9	1018.8	21.29	0.03	00 06 36.34	+39 00 08.6	371
311.6	1944.0	14.29	0.03	426.8	1772.4	15.86	0.03	00 06 36.40	+39 02 37.3	372
299.1	1312.9	17.34	0.04	437.1	1138.5	21.49	0.03	00 06 36.42	+39 00 32.2	373
310.8	2027.2	18.65	0.08	423.1	1855.8	25.18	0.35	00 06 36.44	+39 02 53.8	374
305.6	1961.6	18.07	0.05	420.3	1789.9	19.98	0.03	00 06 36.50	+39 02 40.8	375
305.7	2179.4	18.05	0.05	412.4	2008.5	22.42	0.04	00 06 36.57	+39 03 23.9	376
284.7	1049.0	18.50	0.07	432.3	873.1	23.80	0.10	00 06 36.58	+38 59 39.9	377
294.5	1673.2	19.37	0.15	419.5	1500.0	23.80	0.10	00 06 36.60	+39 01 43.6	378
270.3	591.2	16.25	0.03	434.4	413.2	19.11	0.03	00 06 36.68	+38 58 09.1	379
272.3	684.4	18.92	0.10	433.0	506.7	22.00	0.04	00 06 36.68	+38 58 27.6	380
262.9	754.3	16.03	0.03	421.1	576.6	19.56	0.03	00 06 36.86	+38 58 41.4	381
277.7	1781.9	18.00	0.05	398.7	1608.5	18.82	0.03	00 06 36.92	+39 02 05.1	382
269.3	1497.4	19.79	0.21	400.6	1322.7	24.17	0.14	00 06 36.98	+39 01 08.7	383
274.8	2041.8	18.30	0.06	386.4	1869.2	22.59	0.04	00 06 37.05	+39 02 56.6	384
270.4	2011.8	19.31	0.14	383.1	1839.0	24.22	0.15	00 06 37.12	+39 02 50.6	385
270.8	2064.6	18.38	0.07	381.6	1892.0	21.76	0.03	00 06 37.13	+39 03 01.1	386
240.7	801.9	16.81	0.03	397.1	623.5	19.85	0.03	00 06 37.25	+38 58 50.8	387
246.7	1170.1	18.01	0.05	389.7	993.3	22.45	0.04	00 06 37.26	+39 00 03.8	388
238.5	903.2	16.94	0.03	391.1	725.2	20.87	0.03	00 06 37.32	+38 59 10.9	389
253.3	1743.8	17.05	0.03	375.6	1569.4	20.67	0.03	00 06 37.33	+39 01 57.5	390
257.0	1977.3	16.83	0.03	370.9	1803.9	19.65	0.03	00 06 37.34	+39 02 43.7	391
240.3	1113.0	15.51	0.03	385.4	935.8	16.70	0.03	00 06 37.35	+38 59 52.4	392
242.6	1866.6	18.49	0.07	360.4	1692.3	23.63	0.09	00 06 37.55	+39 02 21.8	393
228.1	1131.9	17.12	0.04	372.4	954.3	18.50	0.03	00 06 37.57	+38 59 56.1	394
232.7	1382.8	18.35	0.06	368.0	1206.3	22.96	0.05	00 06 37.57	+39 00 45.9	395
232.9	1502.2	18.91	0.10	363.9	1326.1	25.04	0.29	00 06 37.60	+39 01 09.5	396
232.9	1764.7	16.39	0.03	354.3	1589.7	20.29	0.03	00 06 37.68	+39 02 01.5	397

Table 1—Continued

$x_{K'}$	$y_{K'}$	K'	$\sigma_{K'}$	x_R	y_R	R	σ_R	α_{J2000}	δ_{J2000}	#
223.6	1372.0	18.05	0.05	359.3	1195.2	23.55	0.08	00 06 37.72	+39 00 43.7	398
231.3	1948.6	17.90	0.05	346.1	1774.2	21.88	0.04	00 06 37.76	+39 02 38.0	399
208.6	945.8	17.81	0.04	359.6	766.9	22.57	0.04	00 06 37.84	+38 59 19.2	400
201.7	1642.7	17.74	0.04	327.5	1466.1	19.11	0.03	00 06 38.17	+39 01 37.3	401
208.8	2320.0	18.45	0.07	310.1	2146.1	23.98	0.16	00 06 38.26	+39 03 51.5	402
186.1	1320.8	18.56	0.07	323.4	1142.5	22.39	0.04	00 06 38.34	+39 00 33.4	403
184.2	1262.9	18.65	0.08	323.6	1084.3	19.84	0.03	00 06 38.35	+39 00 21.9	404
174.3	727.4	16.02	0.03	333.1	546.5	17.51	0.03	00 06 38.36	+38 58 35.8	405
190.5	2020.9	16.50	0.03	302.6	1845.3	20.29	0.03	00 06 38.48	+39 02 52.1	406
190.1	2068.8	18.83	0.09	300.4	1893.4	23.23	0.06	00 06 38.50	+39 03 01.6	407
177.0	1891.5	18.92	0.10	293.7	1714.9	24.20	0.14	00 06 38.67	+39 02 26.4	408
154.4	1311.2	17.98	0.05	292.0	1131.7	20.87	0.03	00 06 38.87	+39 00 31.4	409
121.9	1019.3	17.43	0.04	269.9	837.5	18.99	0.03	00 06 39.34	+38 59 33.4	410
124.3	1604.6	18.99	0.10	251.2	1425.1	23.12	0.06	00 06 39.48	+39 01 29.4	411
104.0	676.6	17.31	0.04	264.4	492.9	20.50	0.03	00 06 39.53	+38 58 25.5	412
114.5	1753.9	18.47	0.07	236.0	1574.7	19.40	0.03	00 06 39.69	+39 01 59.0	413
106.8	1396.0	17.59	0.04	241.1	1215.1	20.72	0.03	00 06 39.71	+39 00 48.0	414
105.0	1476.5	18.66	0.17	236.4	1295.9	26.68	1.36	00 06 39.77	+39 01 04.0	415
90.4	1346.0	19.00	0.11	226.5	1164.4	22.79	0.05	00 06 39.97	+39 00 38.1	416
91.9	1409.3	18.40	0.07	225.8	1227.9	20.36	0.03	00 06 39.97	+39 00 50.6	417
91.2	1916.6	18.15	0.06	206.7	1737.1	19.13	0.03	00 06 40.14	+39 02 31.1	418
80.0	1498.3	17.80	0.04	210.6	1316.8	20.84	0.03	00 06 40.20	+39 01 08.2	419
58.5	1668.0	16.10	0.03	182.9	1486.4	19.32	0.03	00 06 40.62	+39 01 41.8	420
51.6	1431.8	18.57	0.07	184.5	1249.1	24.29	0.16	00 06 40.66	+39 00 54.9	421